20

World Energy Council

CONSEIL MONDIAL DE L'ENERGIE

The Latvian Member Committee of World Energy Council

Jekabs Barkans, Diana Zalostiba

ON THE GLOBAL CLIMATE CHANGE

RTU Publishing House

Riga 2010

UDK 551. 583

Ba 653 g

Jekabs Barkans, Diana Zalostiba. On the global climate change. RTU Publishing House, Riga, 2010. – 88 p.

Annotation

The book, in a popular form, elucidates the problem of the Earth climate change. It considers the causes of natural climatic variations and their character during long-lasting time periods in the past, taking into account the green-house gas effect. The authors estimate, against the background of global heat balance, the influence of heat release by infra-red radiation, considering also the convective heat transfer to the layers of troposphere and stratosphere as well as how this process is affected by carbon dioxide gas. Such an analysis, to a definite extent, would allow the possible character of future climate changes to be judged.

ISBN 978-9934-10-042-0

ABOUT THE AUTHORS

Jekabs Barkans – Emeritus Professor, received the doctoral degree in power engineering in 1963, and the Doctor Habil. degree in power engineering in 1975 (at the Energy institute of Soviet Union Academy of Sciences, Moscow). His employment record includes: a deputy chief operator (1953-1960), and the chief operator of Latvian Power System (1960-1979). Simultaneously, he worked as a docent at the Riga Polytechnical Institute (1964-1979) and since 1980 has been a professor at the Institute of Power Engineering of the Riga Technical University (RTU). He is the laureate of State Price (1970) and of the annual price for scientific results (2004).

His areas of research are: the power system operation; power system control and automation; blackout prevention in a power system and its self-restoration; rational energy utilization; and investigation of riverflows on a long-term scale. He is the author of 20 monographs and test-books, more than 200 publications and 70 patents.

Diana Zalostiba – received the doctoral degree in power and electrical engineering from the Riga Technical University, Riga (RTU), Latvia, in 2010. Since 2006 she has been a researcher at the RTU. Diāna

Zalostiba won the Werner Von Siemens Excellence Award in 2005.

Her research areas include the prevention of blackouts in a power system, its automatic self-restoration; and investigation of the climate change on a long-term scale. She is the co-author of two books, more than 20 publications and 6 patents.

PREFACE

The problem of global climate change is now at the focus of attention in the world. At the same time, it is linked to the issues of environment protection. These, in turn, are so intricate that sometimes doubts can arise as to the advisability to attempt revealing the essence of the problem. Such a position has no future.

In reality, there are good grounds to think that the problem is solvable if we use the existing information on this natural phenomenon. First, it should be made clear that the global temperatures are affected by such a cosmic-scale factor as processes happening on the Sun. For this purpose it is necessary to correlate the variations in the global temperature with solar processes and to find coincidences based on the data of observations.

Obviously, we are restricted in terms of time − because the observations are time-limited. Our possibilities can be extended based on the data of geological explorations. This would inspire hope for revealing the main cause of the climate changes.

Next, the conditions of global heat equilibrium should be clarified. These are dependent on the amount of heat reflected from the Earth. It is known that the Earth reflects heat through three channels: visible light, infra-red radiation, and − inside the atmosphere − by convection. The solution of the problem should be

connected with research into the competition of these channels.

Finally, the situation to a large extent is determined by the greenhouse gases − mainly by molecules of water and carbon dioxide gas, which, reacting to the radiation, create obstacles to the heat release. Making more precise our notion about these gaseous obstructions, we can learn much from them. At the same time, we should take into account that convection has no limitations with regard to the greenhouse gases. Therefore, this channel in the atmosphere plays an active role.

To summarise, it should be noted that the problem has an essentially scientific character. We believe that the aspects, which are comprehensively, and in an understandable manner, considered in this book, may be of interest for wide circles of readers.

The Latvian Member Committee/ WEC express deep gratitude to Professor J.Barkans and his co-author for the dedication of this book to the 85th anniversary of the LMC/WEC.

Through the mediation of the WEC management this book can reach the readers of all the WEC member states.

Dr. Habil. sc. ing. Prof. Namejs Zeltinsh,

President of the LMC/WEC

TABLE OF CONTENTS

INTRODUCTION

The problem of climate change is now at the focus of attention in the world. It is the anxiety of society about the consequences of this phenomenon that has led to great achievements. Despite all that, the nature of this phenomenon is not completely understood. Therefore it is of importance to clear up the relevant facts that are now available.

The work consists of seven chapters. In Chapter 1 the regularities in the riverflows are studied. It is established that the waterflows of many rivers are cyclic in character; therefore, applying the discrete wavelet analysis to these cycles and comparing them with the cycles of solar intensity variations we can reveal similarities in both cases; this indicates the determinative influence of the Sun.

Chapter 2 presents a continuation of the analysis as related to the global climate changes. Here also the dominant influence of the Sun has been established. Taking into account that the observation time for the cycles of solar processes is only 300 years, the data on the paleo-temperatures have been used that were obtained while studying the ice cores from Greenland and Antarctic glaciers. This made it possible to substantiate the climate changes based on the data of past ages.

In Chapter 3 the Earth heat equilibrium is considered. Chapter 4 deals with the heat reflection by radiation while Chapter 5 – with the heat reflection by convection. Chapter 6 considers the carbon dioxide equilibrium; finally, Chapter 7 discusses the temperature change associated with carbon dioxide.

It is possible to generalize the temperatures on the Earth under the condition only that all the solar heat reflected from it into space is twice as large as that allowed by the carrying capacity of the channels for the infra-red heat radiation, which is limited due to absorption of greenhouse gases. Within the atmosphere this could only be provided by vertical convection flows, which are not affected by the absorption "windows" for greenhouse gases. The heat from there is delivered to the upper atmosphere layers not containing water molecules, and then is practically dispersed at the IR wavelengths corresponding to the cooled media. The convection, in compliance with the physical laws, reduces the natural temperature changes, creating with respect to them a stabilising negative feedback (thus being a stabilising factor).

CHAPTER 1.
CAUSES OF GLOBAL CLIMATE CHANGE

1.1. Investigation into the river waterflows

When analysing the cyclic processes we tried to find out the factors underlying them. The waterflows of rivers, being the result of climatic peculiarities, were found to be an appropriate matter for scientific inquiry.

We therefore proposed and mathematically substantiated an approach that widens, to an extent, the existing views on the dynamics of climate change. In the studies of river waterflows the integral series of their deviations from the average values were employed [1]:

$$Q_n = \sum_{i=1}^{n} q_i - q_{av} \ , \qquad (1.1)$$

where q_i, q_{av} denote the current and average water flows; i is the order number of a term, $i = 1,2...n$; n is the length of time series.

The integral series were involved since this allowed us to smooth the individual annual spikes on the curves describing cyclic processes thus achieving a greater visuality.

To study the phenomenon of river waterflow cyclic changes the Fourier's analysis was used. At this stage, an attempt was made to assess the methods applied in this inquiry as to their optimality for achieving the set purpose. When analyzing this phenomenon, we tried to

understand its character. With this in mind, we decomposed it into components and studied all of them and each separately.

The current annual values of the Daugava integral series are displayed in Fig.1.1 [1], where curve (1) shows the interal function, (2) is the approximating curve; curves (3), (4), (5) stand for 84-year, 30-year, and 11-year cycles, respectively.

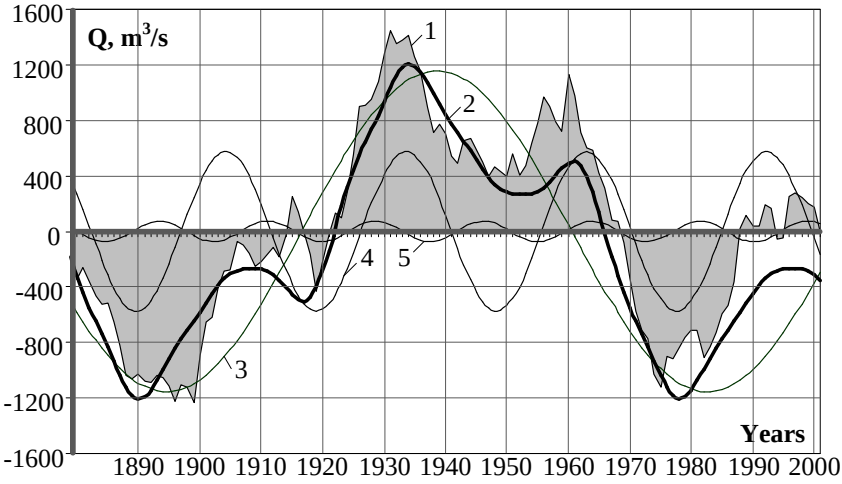

Fig.1.1. The integral function (1) and approximating curve (2) of Daugava waterflow; componets: 84-year (3), 30- year (4), and 11-year (5) cycles

In the next stage of the analysis, the wavelet transform was used, which is well suited for studying the structure of non-uniform processes [2], [3].

1.2. Wavelet analysis of cyclic processes

The wavelets are specific functions in the form of short waves with the zero integral value and localization along the independent variable axis, which are capable of shifting along this axis and scaling (extension and contraction). At analyzing the process, owing to changes in scale, the wavelets are able to reveal the dissimilarities in the process characteristics on different scales; whereas through shifting, its properties could be analyzed at various points over the whole interval under study. From different wavelet transform types, for our purpose we chose the wavelet technique using the advantages of a continuous wavelet transform (CWT) and a fast discrete wavelet transform (DWT).

Continuous Wavelet Transform

When CWT is applied, the wavelet coefficients are calculated by transforming the basic integral formula into a sum, since the time series are composed of discrete magnitudes [2], [4]:

$$W_A\ a,b\ = \frac{1}{n\ a,b} \sum_{k=0}^{N-1} q_k \psi^* \left(\frac{t_k - b}{a} \right), \qquad (1.2)$$

where $\psi\ a,b,t$ are wavelets scaled to the "mother" function $\psi\ t$ and are its shifted copies; a is the scale (determines the wavelet size); b is the shift (specifies the wavelet localization); * is a complex conjugation; $q_k = f\ t_k$ are the values of time series function with

step Δt, where $t_k = k\Delta t$ (k being the order number of the term, $k = 0,1\ldots,N-1$); N is the length of time series. The function $n\ a,b\ = \sum_{k=0}^{N-1} e^{-\frac{1}{B}\left(\frac{t_k - b}{a}\right)^2}$ allows balancing the output data participating in calculations for differently scaled values of coefficient a. For the Morlet wavelet $B = \alpha^2$, where parameter α defines the Gaussian width by which the flat wave of a wavelet is modulated. Usually $B = 2$.

To estimate the influence of differently scaled components on the resultant process the spectrum of local energies (or scalogram) is used:

$$S\ a_i, b_j\ = \left| W_A\ a_i, b_j\ \right|^2. \qquad (1.3)$$

Employing (1.3) the global energy spectrum (called scalegram function) can be calculated[1]:

$$G\ a_i\ = \frac{1}{N^*} \sum_j S\ a_i, b_j\ , \qquad (1.4)$$

where N^* is the point set used for calculation of mean value (s).

Discrete wavelet transform

In the next stage of our analysis the so-called discrete wavelet transform is used as follows [1], [4]. In each step the process identity divided into two components: rough (approximating) and precise (detailing); this latter,

[1] function (1.4) also is callded wavelet variance [3]

in turn, is divided into two groups in the next iteration, and so on. In the work, a fast wavelet transform with Mallat's pyramidal algorithm is used, with the frequencies divided by half in the signal (data of time series) frequency range. This algorithm allows applying two type filters for signals: low frequency Lo and high frequency Hi, to the inputs of which the signal $s\ t$ is fed. The Lo filter isolates low frequency $|\omega| \le \pi/2$ and provides frequency representation A_i for approximation of the signal, and the Hi filter does the same for high frequency $\pi/2 \le |\omega| \le \pi$, providing its representation D_i for refining the signal as shown in Fig.1.2.

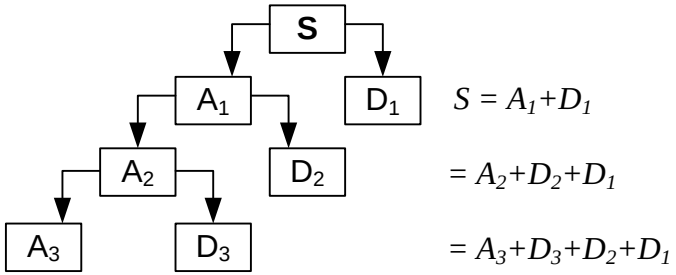

Fig.1.2. The structure of signal reconstruction

In the next iteration, using Lo and Hi filters the low frequency component A_i is again divided into two ones: A_{i+1} and D_{i+1} thus forming a wavelet-filtering system that performs decomposition of the signal into components

(Fig.1.2). As the result, the complete set of approximating and detailing components is obtained. By summing up all the components of a process the initial signal is reconstructed.

1.3. Wavelet analysis of the river waterflows

The results of CWT analysis are shown in Fig.1.3 for waterflows of the Daugava river.

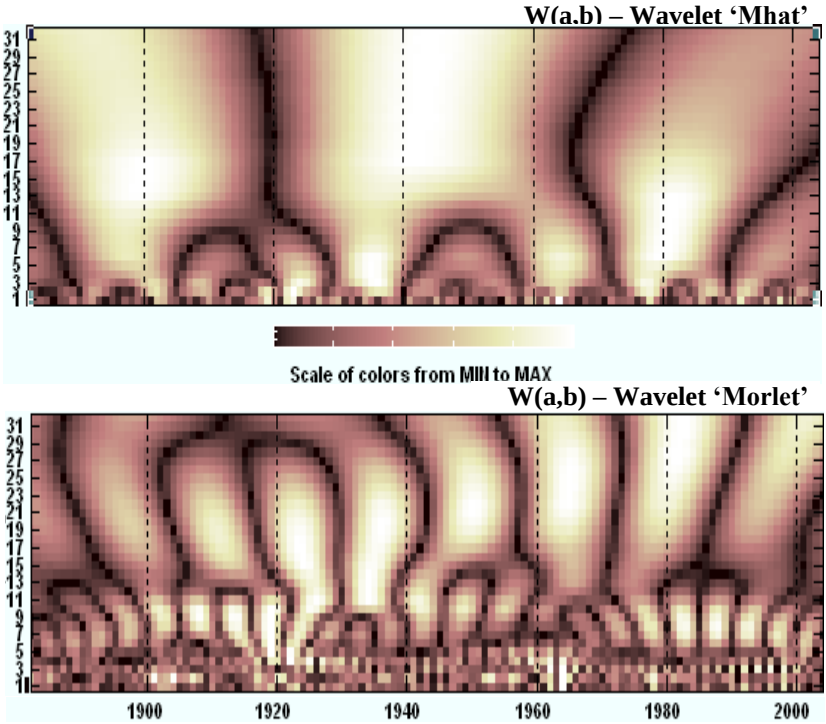

Fig.1.3. CWT of the Daugava waterflow: 1 – the integral function; 2 – using wavelet 'Mhat'; 3 – using wavelet 'Morlet'

Depending on the wavelet used, the results can be detailed in the area of low (1) or high (2) frequencies.

Since it is important to find out the specific weight of components in the process, we will calculate the global energy spectrum by (1.4). Fig.1.4 shows that, using continuous wavelet transform for waterflow, the main cyclic components with approximately 10-, 29-, 40- and >84-year periods can be isolated. The last of the above listed periods is to be defined more precisely, since the function line for long periods (low frequencies) has not reached the maximum variance point.

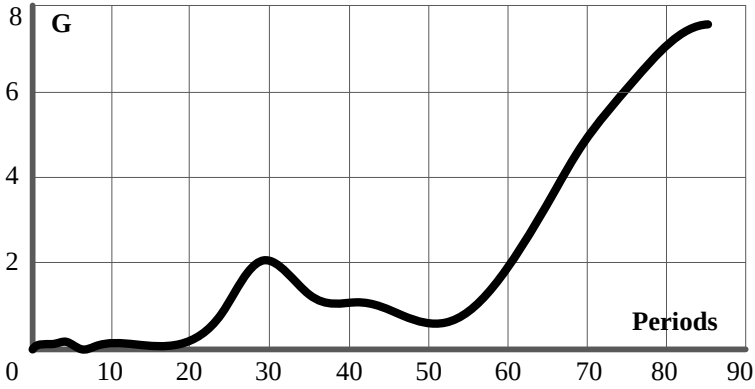

Fig.1.4. The global energy spectrum for Daugava (scalegram)

The result of descrete wavelet transform for the Daugava waterflow integral process is shown in Fig.1.5, where the same cyclic tendencies that are revealed that are seen in Fig.1.3 (obtained by CWT).

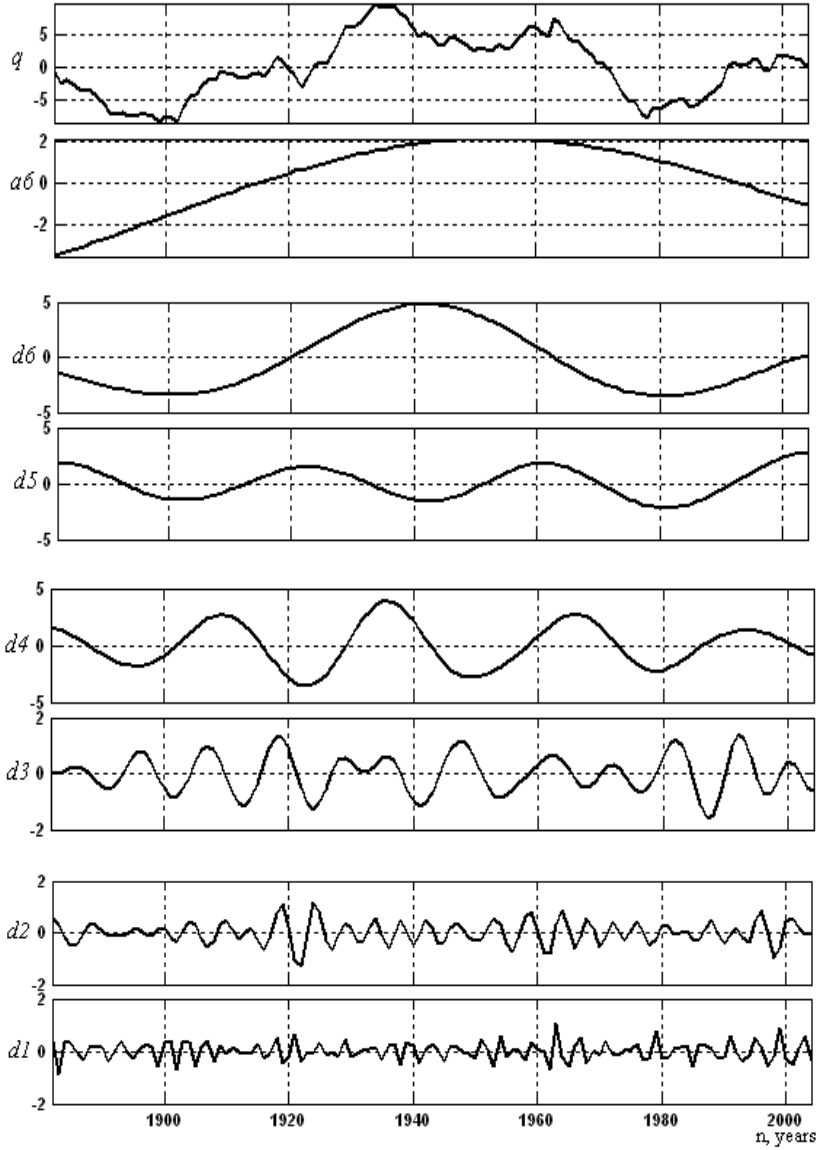

Fig.1.5. Discrete wavelet transform of the Daugava waterflow integral series

The 1st and the 2nd levels (d_1 and d_2) in Fig.1.5 correspond to the peculiarities of the process that probably influence (maybe only slightly) its regular character [3- 10]. The levels of particular interest are d_3 - d_6. The 3rd (9-13 year cycle) is similar to the known 11-year cycle of the Sun. At the d_4 (28-30-year) and d_5 (39-41-years) the so-called Bruckner cycle[2] appear [5].

In turn, the centenary cycles correspond to the d_6 components with 80-82-year periods. The last level, a_6, presents a fragment of less than half-period of this cycle. In further analysis it is worthwhile to juxtapose the components having the largest specific weight with other cyclic phenomena that could be their cause.

1.4. Solar cycles

Solar activity is a periodic process of appearance and development of active regions (sunspots) which are actually visual manifestations of tangled magnetic fields on the Sun. The temperature in such places is approx. 1500÷2000°C lower than on other surfaces, which allows discerning them by colour [6]. The sunspots have a comparatively short duration (one month on the average).

The idea of computing sunspot numbers was originated with Rudolf Wolf in 1849 (Zürich), Switzerland. He

[2] 30-year climate cycles described in 1890 by Bruckner − a German scientist who studied glaciers of Switzerland and riverflows of Russia [2]-[3]

proposed characterizing the state of solar activity by a relative number of spots, which usually occur in compact groups. The combination of sunspots and their grouping is used because it compensates for variations in observing small sunspots. The Wolf numbers are determined based on the monthly average 24-hour observations [7]:

$$W = k\ (10g + f)\ , \qquad (1.5)$$

where g is the spot group; f is the number of individual sunspots, k is a factor that varies with location and instrumentation (also known as the observatory factor or the personal reduction coefficient K).

The processes on the Sun have regularly been observed since 1700 (see Fig.1.6, [8]), which allows, to an extent, their running to be judged.

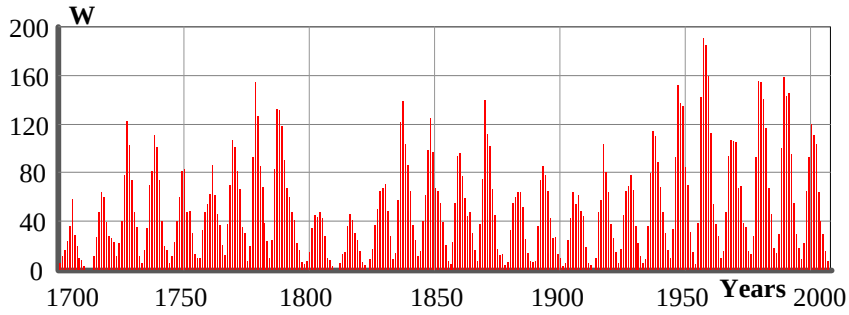

Fig.1.6. Solar activity in theWolf numbers

In our analysis we will consider first the well-known 11-year solar cycles. A peak in the sunspot count is called "solar maximum". The time when few sunspots appear is

called a "solar minimum". The activity rises in 4-5 years and falls in 6-7 years. The duration of a period can vary within 9-14 years.

To verify the hypothesis that the influence of solar activity on the processes occurring in the Earth atmosphere is responsible for the cyclic processes, we have performed the wavelet analysis of the Wolf numbers for 300 years of observation [9]-[11].

The global spectrum is shown in Fig.1.7. Could be expected, the 11-year cycles are of the greatest specific weight. In the figure, also other cycles can be seen in a wave-like form: 52-, 102- and ~188-year cycles.

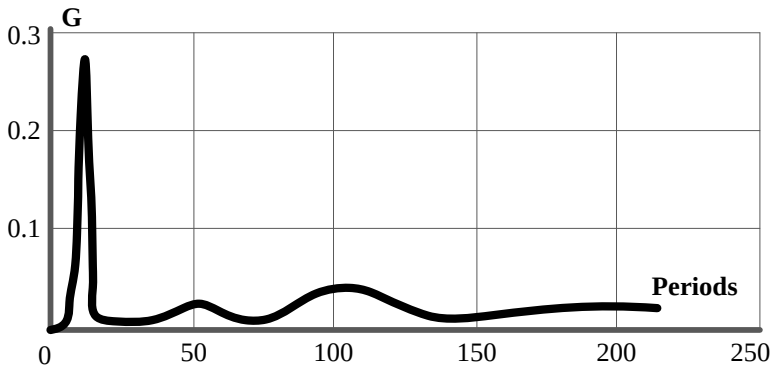

Fig.1.7. The global energy spectrum of Solar activity

The discrete wavelet transform of solar activity is shown in Fig.1.8.

The considered above 11-year cycles refer to level d_3. The 25-year and 100-year cycles are also well-known.

the components of the process the initial signal is reconstrucned. The discrete wavelet transform of solar activity for bigger`s and low frequency`s is shown in Fig.3.

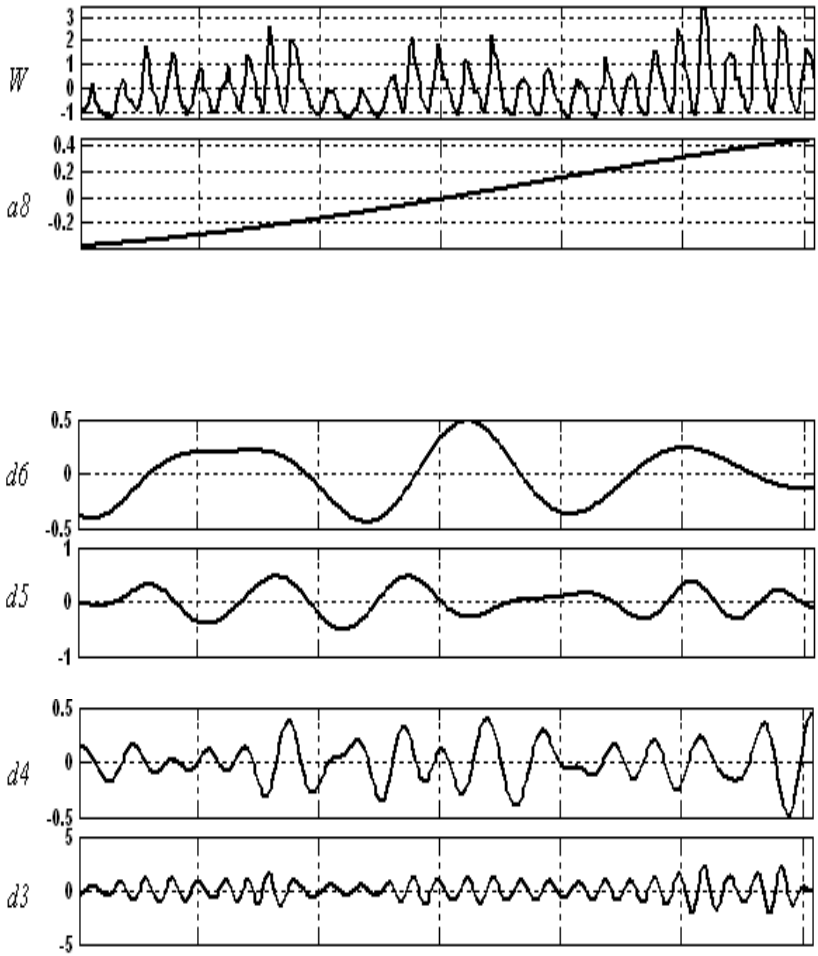

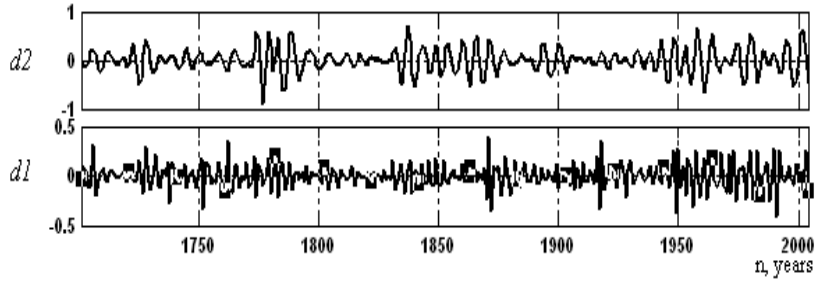

Fig.1.8. The discrete wavelet transform of sunspots

Of particular interest is the component a_8, which presents a fragment resembling a half of the semi-period. If such a cycle exists, its duration can be on the order of 1000-1200 years. We cannot verify this directly, since there are no relevant long-term observation data. However, we can look over the "brink" using indirect possibilities. The lower frequencies are to be defined more precisely in the future, since the observation data available so far are insufficient. In other words, this problem can be solved based on the similarity of the processes observed for some other objects that can be considered influential.

1.5. Geomagnetic index of the Sun

Another parameter of the solar activity that can be used for its characterization is the geomagnetic index (designated by aa_R in Fig.1.9) [7], established since 1870. We can see that this index also possesses a cyclic character, and that it also contains low-frequency and high-frequency components. The aa_I index is the

geomagnetic component that repeats the aa_R index with a shift of several (about 4-5) years.

Taking into account that the solar activity is used for analyzing the river waterflows, the methods for forecasting this parameter are needed. NASA have developed several methods for forecasting the maximum solar activity, $W_{\max}$, that is expected in the next *n*-th 11-year cycle based on the data for the (*n*-1)-th cycle.

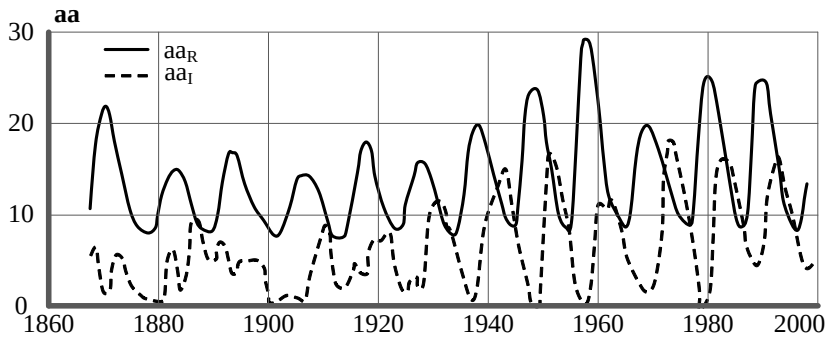

Fig.1.9. Geomagnetic index of solar activity

The most precise method based on the retrospective forecasting uses the Wolf numbers and geomagnetic parameters. The corresponding regression equation can be written as [7]:

$$W_{\max}\ n\ = 19.8 + 0.452 DD\ n-1\ - W_{\max}\ n-1\ \pm 16.8 \quad (1.6)$$

where $DD\ n-1$ is the number of geomagnetically turbulent days in the (n-1) cycle; $W\ n$, $W\ n-1$ are the

Wolf numbers in the succeeding and previous cycles; $DD \geq 25$.

The coefficient of correlation between the relationships is $R = 0.97$.

1.6. Time variations in global temperature

The view of existing tendencies in climate changes proposed by the authors is based on the available facts (Fig.1.10) [12]. Earlier [1], the cyclic behaviour of the world's riverflows was discovered, which was found to correlate with the cycles of solar activity. Similar correlation was revealed by the authors for global temperature anomalies.

As is seen in this figure, in the period of 1850-2007 the temperature maximum was reached in 1998.

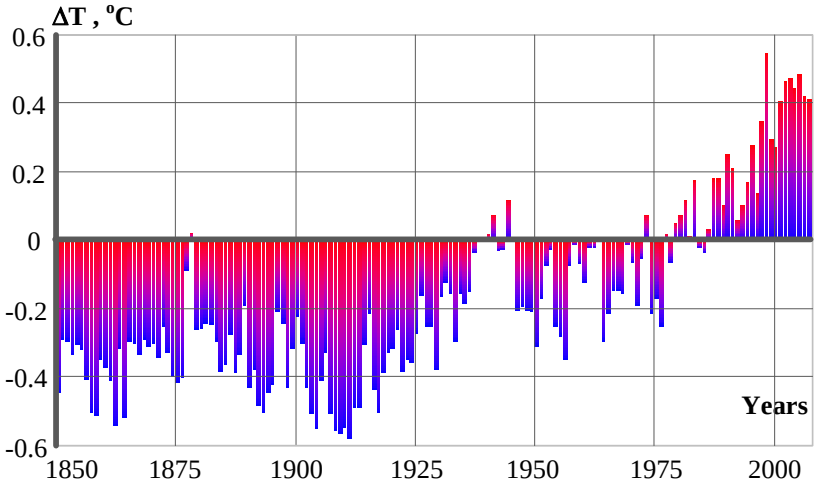

Fig.1.10. Global mean surface temperature anomalies in 1850-2007 relative to 1961–1990

Variations in the CO_2 content of terrestrial atmosphere and in the global mean temperatures as correlated with other factors are shown in Fig.1.11 for the period of 1800-2000, where curve (1) shows the world's population, (2) – emission of CO_2, ‰ ; (3) – energy production (10^9 toe); (4) – global mean temperature anomalies relative to 1961–1990.

The authors stress that the processes of global climate change are of ambiguous character, since they consist both of the natural and the anthropogenic components.

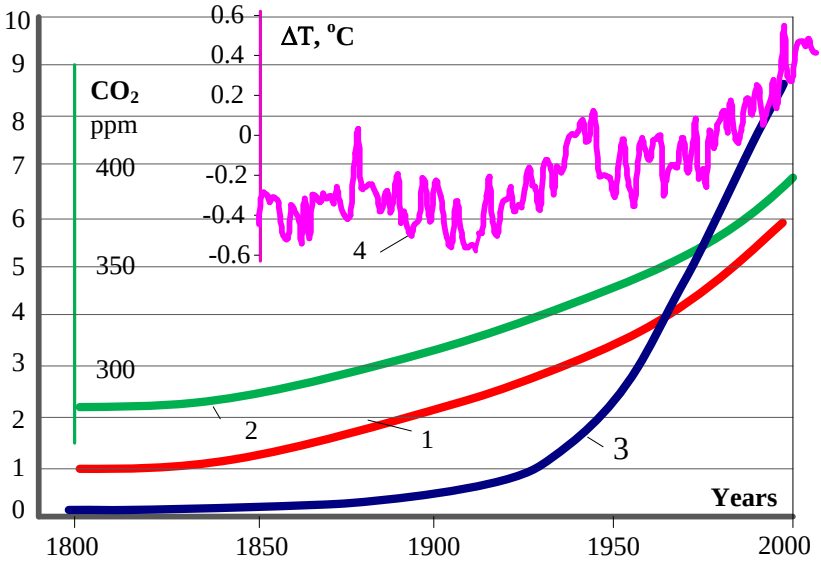

Fig.1.11. 1 – the world population (10^9); 2 – emission of CO_2, ‰; 3 –energy production (10^9 toe); 4 – global mean temperature anomalies relative to 1961–1990

At analysing by analogy the global temperature variations, some unclear points arise that should be decoded, such as [10-11]:

1. Why are harmonic fluctuations observed in the process of temperature change?

2. What was the cause of the interruption in temperature rise in the 50-70-ies of the past century?

3. How fast does the global atmosphere respond to the processes going on the Sun?

4. How could the start of temperature rise in 1910 be explained when there was no anthropogenic effect of huge carbon dioxide emissions (Fig.1.11)?

5. What does the long-term fragment of solar cycle (in 300 years of observation, resembling a semi-period's half)' mean?

1.7. Comparison of the DWT components

To study the cyclic natural processes, the discrete wavelet analysis turned out to be the best.

The results of the analysis related to the temperature and solar activity variations are shown in Fig.1.12. The temperature cycles characterized by $d_3 \div d_7$ components evidence that the temperature response of the Earth atmosphere to the solar processes is practically simultaneous (on the global scale). Meanwhile, the following peculiarities were noticed.

For the year of 1910 a temperature phase change to the opposite can be observed. This could be explainable by the phenomenon of re-magnetization, which lends support to the role of the magnetic field variations. However, the temperature is affected in the same way as before the phase inversion. Possibly, this explains the temporary temperature fall in the 1950-1980-ies, when the centenarian and smaller cycles of the solar activity came into anti-phase, while for the cycles of greater periods the in-phase property held. The relationship between the solar temperature and activity phases is now

gradually, within 55 years, returning to the in-phase state. It is difficult now to understand all that completely, therefore this should be the subject for further investigation.

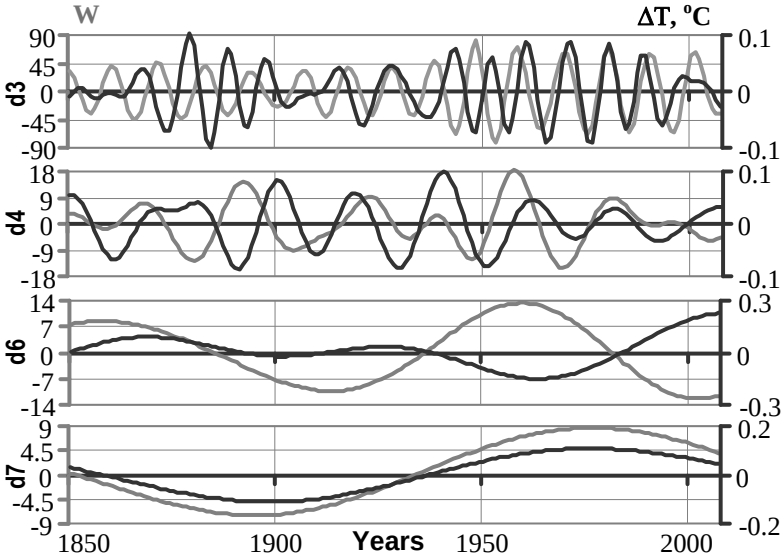

Fig.1.12. Comparison of wavelet transform components for solar activity (grey lines) and global mean temperature anomalies (black lines)

CHAPTER 2.
THE MILLENARY CYCLES OF CLIMATE CHANGE

2.1. The 1000-year cycle

As was shown above (Fig.1.8), at analyzing solar activity data on the last curve (a_8) a half of one semi-period could be seen, which possibly is the fragment of a 1000-year cycle. Unfortunately, the time of observation was insufficient to define their shape more clearly. Therefore, to clarify the situation and answer the remaining questions (defined in Ch.1.6), the data for longer time spans were needed. So we tried another approach: to find relationships between the solar activity and global temperatures in the inverse problem − that is, to judge the solar cycle from the data on past temperatures.

A more accurate account of 1000-year climate changes was obtained studying the ice cores from Greenland glaciers in the places where snow remains unthawed in summer. It is known that a glacier is the pressed snow, which at its re-crystallization transforms into ice. In the millennial ice cores the annual layers could well be discerned. These layers are separated from each other by summer and winter sediments, which have different structure, density, and dust composition (depending on the season). All these differences should not present any problem for several last millennia; however, in deeper

horizons these layers are fused under the influence of pressure, and the dating becomes more complicated and less precise [**Error! Reference source not found.**].

In the stage of ice formation the air becomes stored in bubbles. Therefore to isolate it from the ice core the data on the atmosphere composition and climatic conditions of that time are needed. In the atmosphere, apart from simple hydrogen and oxygen isotopes ^{1}H and ^{16}O, there are contained in minor quantities heavy isotopes ^{2}H and ^{18}O. It turns out that between the specific weights $^{2}H/^{1}H$ and $^{18}O/^{16}O$ (designated by $\delta\,^{18}O$ and $\delta\,^{2}H$ and expressed in promiles, ‰, with respect to the SMOW (standard mean ocean water)) and paleo-atmospheric mean temperature a linear relationship exists [13-16]. Thus, for example, a 1‰ decrease in $\delta\,^{18}O$ indicates a 1.5 ^{o}C temperature fall, while 6‰ decrease in deuterium ($\delta\,^{2}H$) – a 1 ^{o}C temperature reduction. A good correlation between these values is found also in other investigations, which provides grounds to consider the glacial cores of Greenland as a natural monitor of temperature fluctuations. A smoothed (in 50 years) diagram of Fig.2.1 [17, 18] presents the GISP2 ice core data (Greenland) for the last 5000 years. The points 1 and 2 at Fig.2.1 correspond to temperatures changes $\Delta T_1 = 0.1^{\circ}C$ and $\Delta T_2 = -0.55^{\circ}C$ in Fig.1.10.

The behaviour of temperature variations explains the character of the fragment that resembles a half of the semi-period for 300 years presented above (in Fig.1.8),

which, as was suggested, can have a period on the order of 1000 years. This turns out to be an essentially steep temperature rise − though comparatively short-term on the scale of millennia − which really repeats in the form of a millenary cycle (Fig.2.1).

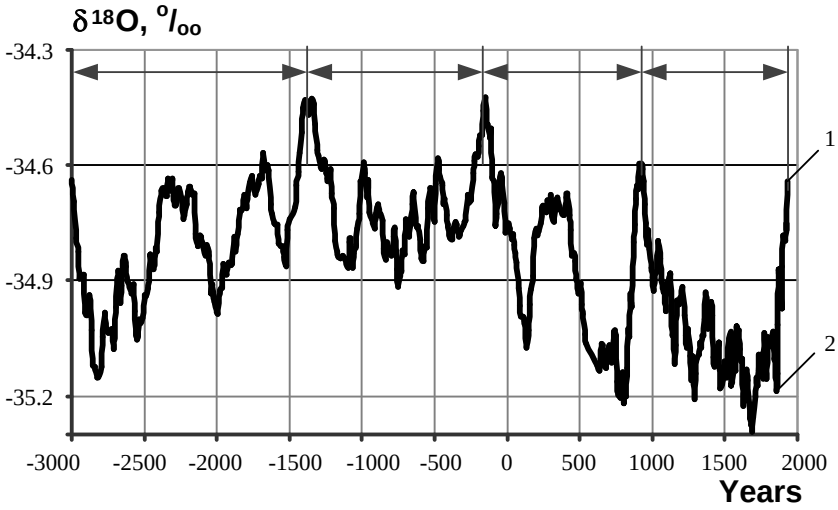

Fig.2.1. Distribution of oxygen $\delta^{18}O$ isotope in the upper layers of GISP2 ice cores (the values are smoothed in 50 years)

The character of temperature variations arising under the influence of processes going on the Sun obeys definite regularities. To reveal them, the five thousand years belonging to the last inter-glacial period are divided into four sub-periods.

During the first − between 3000 and 1600 BC − the temperature was noticeably rising. During the second

sub-period − 1600-200 BC − the temperature stabilized at a higher level.

During the third − between 200 BC and 900 AD − the temperature fell markedly; in the end, during the last sub-period, there was an additional temperature decrease, which gave to it the name “small glacial epoch”.

The mentioned millenary spans are bounded by steep short-term temperature rises lasting approximately 150-250 years (Fig.2.2). Thus, for example, during the first span, which, as distinguished from the other millenary was lasting 1600 years, these intermediate temperature rises are expressed the most clearly. They are less distinctive in the last millenium, which turned out to be the coldest.

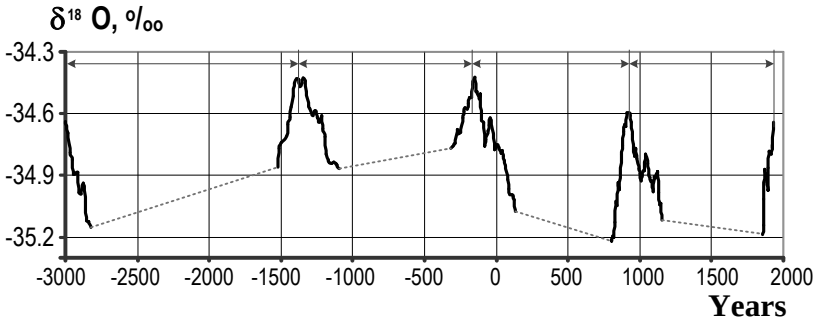

Fig.2.2. Extremal temperature variations within the millenary cycles

When applying the wavelet transform some problems arise with the use of standard spectral filters. The matter

is that the millenary spans, as already mentioned, are bounded with characteristic steep and short-term (150-year long) regularly repeated temperature rises. Conventional filters do not sense this regularity, and relate these variations (peaks) to the components of so-called high-frequency processes; this is obviously erroneous. To make a relevant analysis, we need a filter (with recurrency elements) that, despite the extremal temperatures being short-term, is able to "discern" their specificity and relate them to a low-frequency process described by a U-shaped curve.

The maximal temperatures were in 1400 BC and the second BC sub-period. In our era, the maximal temperature was in 1998 − by 0.2°C smaller than in the X century.

The wavelet transform estimates of slower changes are quite adequate and very interesting. These are shown in Fig.2.3.

At the d_4 level steep extremal temperature rises are observed, which are „maintained" by the in-phase temperature changes in 200-500-year cycles.

At the d_6 level one can see the rise in temperatures early in the five thousand year period, their stabilization during the 2^{nd} millennium, and then, during the two thousand year period – their fall.

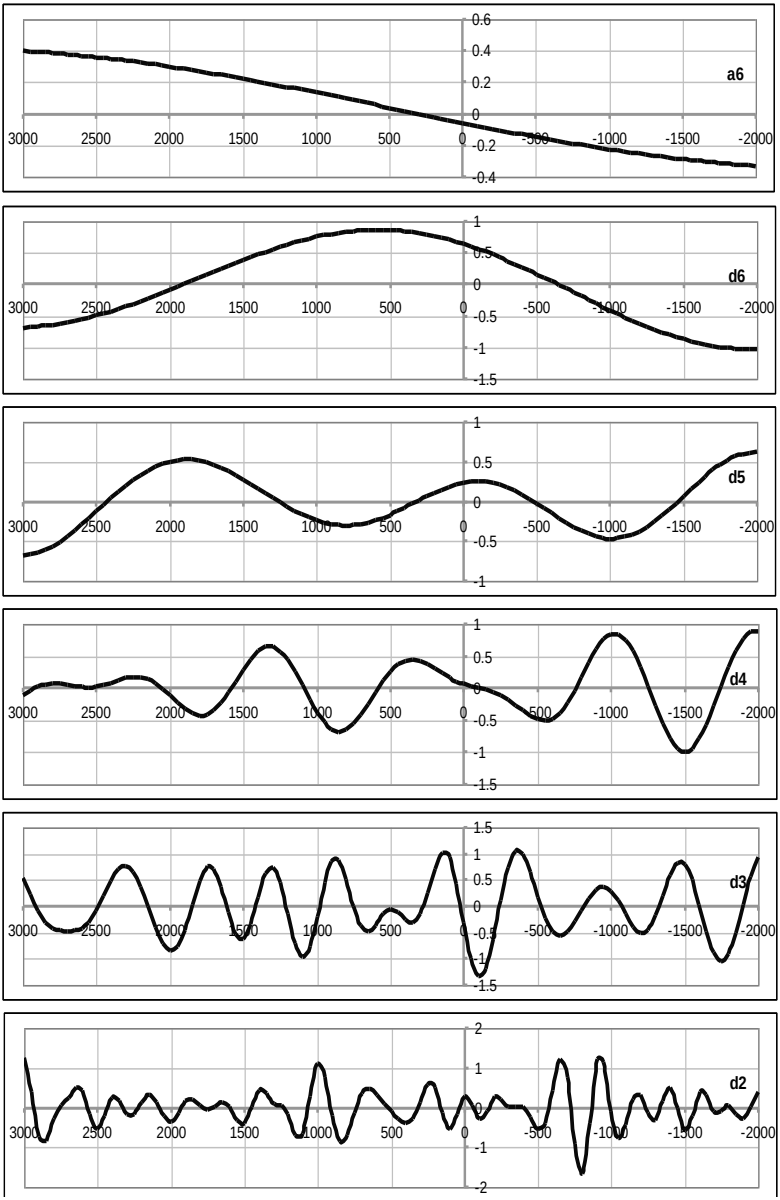

Fig.2.3. The wavelet analysis of 5000-year period

It is clear that at the peak of extreme temperature rises during the inter-glacial epochs the temperature first is increasing and then decreasing before a next ice-up had burst out.

The a_6 level indicates a monotonical tendency towards a long-term cold spell.

2.2. Historical and archaeological evidence of temperature variations on a millenary scale

Historians and archaeologists have received irrefutable facts concerning the events related to paleo-temperature variations [10], [11], [17]. Thus, for example, it is known that 2800 years BC an ancient Egyptian kingdom (being famous with its pyramids) completely disappeared. Archaeologists found out that Egypt then suffered a humanitarian catastrophe caused by Nil's being dried up due to unusually low temperatures (shown in Fig.2.1 and Fig.2.3). This fact was confirmed by archaeological excavations as well as by investigations of stalactites. It is now established that at those times the thawless Atlantic icebergs reached the latitudes of Africa.

The maximum temperature peak in the last interglacial period was reached during the reign of Ramsesses the Great (a pharaon of Ancient Egypt).

In the X century a Vikings' expedition reached an ice-free land, which was named by them Grenland (a green

land). Fig.2.1 and Fig.2.3 data convincingly show that the time of Vikings' expedition exactly correlates with an extreme temperature rise which lasted for about 50 years – i.e. a period long enough for glaciers to thaw. Another expedition arrived at some other land and called it Vinland (now Newfoundland).

Later on, in the XIV century one more expedition departed for Greenland to visit their ancestors, and this time there was a kilometre-high glacier, with no traces of man revealed.

In this figure also the XVII century – the coldest time of "a small ice period" (XII–XVIII) – is clearly seen. At those times in Europe, owing to severe cold, bad harvests occurred, which were followed by famine, plague, and other calamities. The last millennium in these 5000 years was the coldest. Population of that time suffered mostly from the cold.

2.3. Hypotheses employed for explaining the interrelation of the processes

Insufficient understanding of the physical processes caused by the interplay between those occurring on the Sun and the observed climate change sends us in search of acceptable hypotheses. Two of them deserve especial attention.

According to the first, in the atmosphere the trajectories of cosmic radiation particles undergo variations caused

by the interaction of solar and global magnetic fields. These particles act as the centres of condensation for atmospheric water vapours (much like as it occurs in a Wilson`s chamber), which, in turn, affects the global temperature.

According to the second hypothesis [14], the global temperature variations are the result of minor changes in the radius of the Sun corresponding to its activity cycles. Possibly, both the factors are influential.

2.4. The long-term climate changes

The data on the ice cores (Vostok) (1) and the ocean sediments (2) made it possible to reconstruct the temperatures for 600 thousand years, which are shown in Fig.2.4 [6, 19].

In this figure we also can see the above mentioned (Ch.2.1) U-like behavior of the temperature changes with rare and short-term extreme temperature rises against the background of low temperatures. During these 600 thousand years there were six glacial epochs, about 100 thousand years each, with short (approximately 10–20 thousand years) interruptions.

The extremal paleo-temperature variations and their smoothed representation during the last 420 thousand year are shown in Fig.2.5 and Fig.2.6.

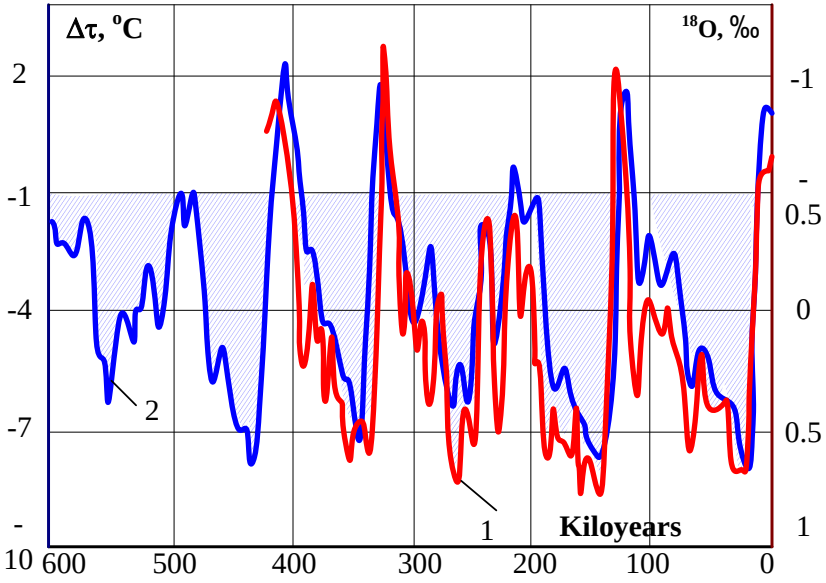

Fig.2.4. Relative temperature deviations during glacial epochs: (1) - temperature deviations in Antarctic (Vostak data) and (2) oceanic calcite oxygen isotope $\delta^{18}O$ data

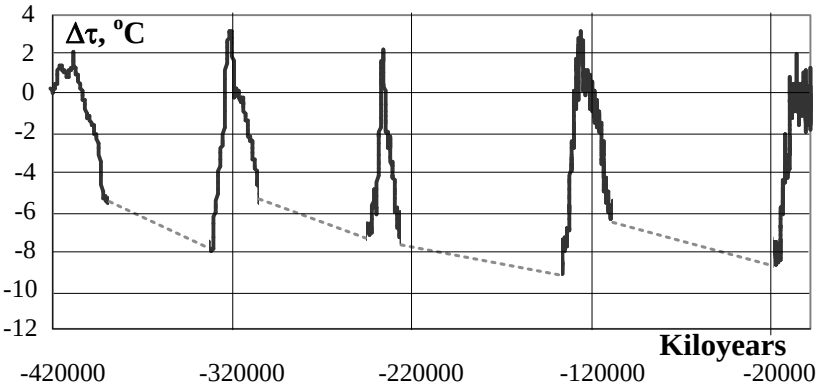

Fig.2.5. Extremal paleo-temperature variations

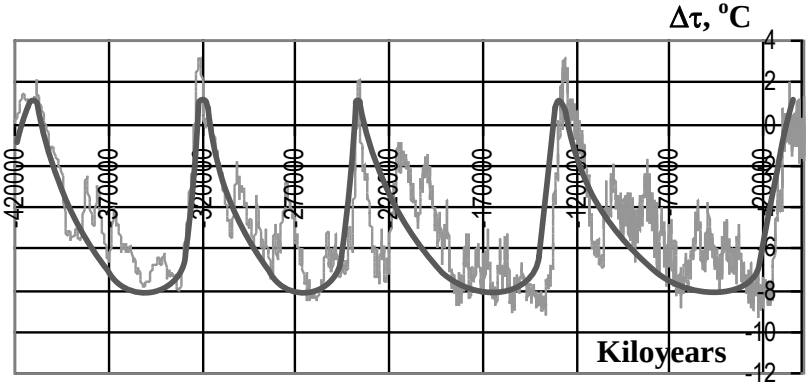

Fig.2.6. A smoothed representation of the extremal paleo-temperature changes

In contrast to the thousand-year cycles, where the temperature variations reach 1-2 ºC, in glacial periods the changes are 7-9 ºC.

To explain the causes of glacial periods, a Serbian geophysicist, M.Milankovitch, proposed an astronomical hypothesis of the climate changes. According to this hypothesis they are affected by three factors: the eccentricity of the Earth orbit; tilting of the Earth axis to the ecliptic plane; and the longitude of the perihelion of the orbit (the minimum distance from the Sun) with respect to the moving vernal point.

At the same time, there are so many solar activity cycles − and not exceptional ones − that coincide with the temperature phenomena. However, since there is an abundance of superimposed solar cycles, another

explanation is difficult to exclude: presence of the cycles corresponding to glacial periods.

Is there any sense in consideration of the cycles whose duration exceeds thousands of years? Probably, yes; at least, this would be interesting, because the shape of such a long-term period correlates with the processes considered in Ch.2.2.

The corresponding wavelet analysis is reflected in Fig.2.7, where the data for a 420-thousand-year period (in kilo-years) is presented.

The last glacial epoch ended aprox. 15000 years ago.

The most characteristic feature of glacial epochs is long-lasting high-frequency processes, which are adequately described by the wavelet analysis. In Fig.2.7 component d_6 relates to the temperature minimum periods, and shows mainly 14000-year cycles; d_7 corresponds to 24000-year cycles and inter-glacial epochs. Now, when the end of our inter-glacial epoch is due, these periods are of particular interest.

On curve d_8 a fragment of 100-thousand-year cycles could be seen, while on d_9, d_{10}, and a_{10} curves − even longer cycles. The trend of curve a_{10} evidences that at the beginning of a 420-thousand-year period the global temperature was decreasing monotonically, and then, during the last glacial period, it has increased.

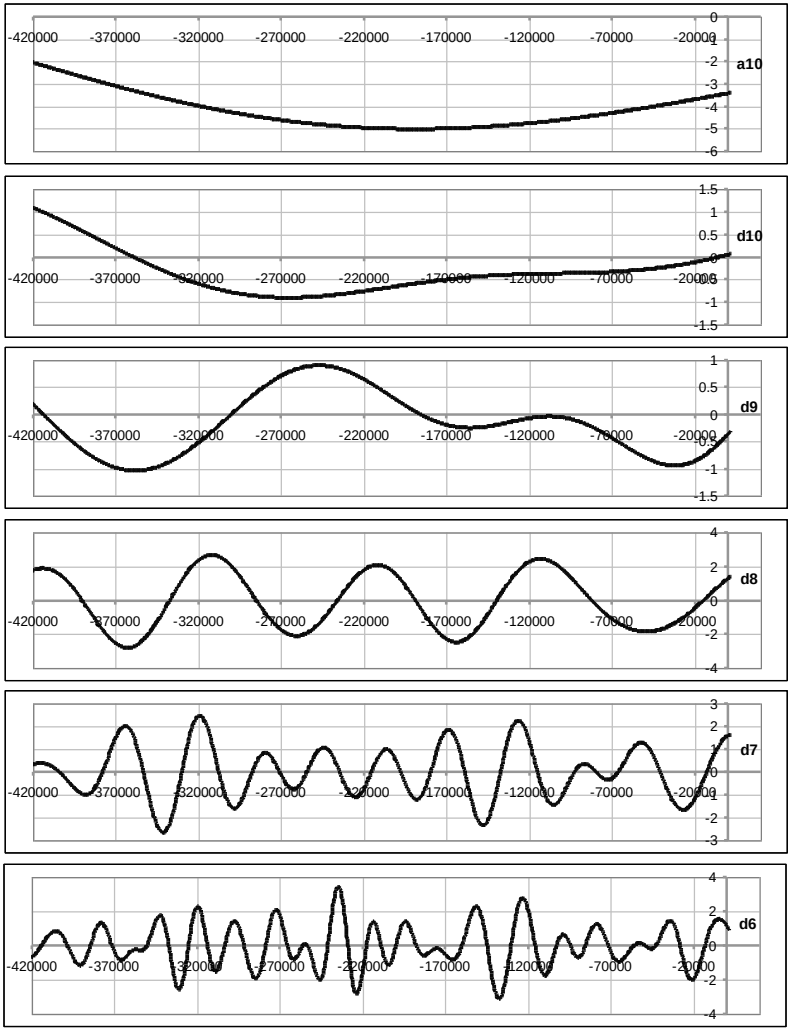

Fig.2.7. The wavelet analysis of 400 thousand year period

CHAPTER 3.
THE CONDITIONS FOR THE GLOBAL TEMPERATURE EQUILIBRIUM

As is known, the Earth receives heat from the Sun mainly in the visible light and short-wave infrared regions (Fig.3.1). Through cosmic space the heat can only be transferred by electro-magnetic radiation.

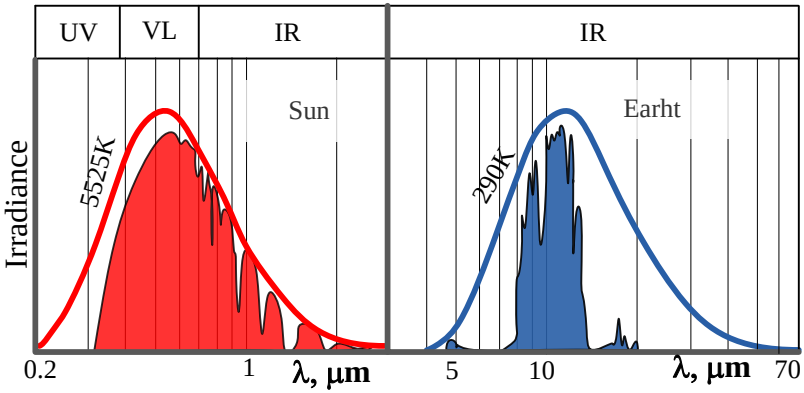

Fig.3.1. Solar radiation (left) and thermal radiation (right) spectra

In turn, the Earth returns the heat to the space in three ways: with immediate reflection of the light, by radiative and by convective channels. The global heat is transmitted in the 4-70 μm wavelength region of IR radiation (Fig.3.1).

3.1. Reflection of the Earth heat

By infrared radiation the heat is partially reflected through the troposphere – the lower part of the atmosphere at a height of 8–10 km in the temperate latitudes and of 16 km in the equatorial zone (Fig.4.7). In this tropospheric zone, besides the nitrogen and oxygen there also exist water vapour in its lower part (an 8-10 km high layer), carbon dioxide, methane, ozone and some other gases that react with the infrared radiation.

At the temperatures -50ºC that exist in the upper layers (strata) of troposphere and the lower part of stratosphere, the radiation shifts towards a longer wave region (Fig.3.2).

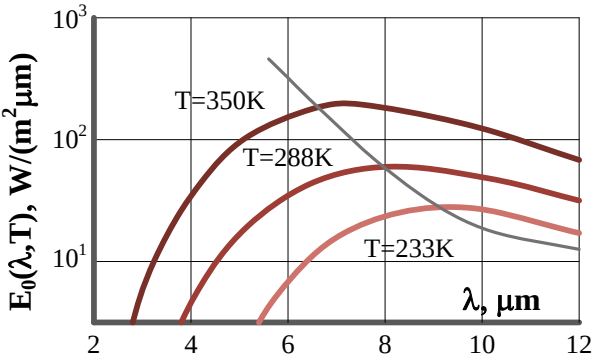

Fig.3.2. IR radiation wavelengths *vs.* temperature

The wavelength corresponding to the maximum radiation E_{max} at the absolute temperature T is found from the Winn relationship:

$$\lambda_{\max} = b / T, \qquad (3.1)$$

where $b = 2.8978 \cdot 10^{-3}\,\mathrm{m} \cdot \mathrm{K}$.

3.2. Global heat balance

The global temperature equilibrium is determined by the solar energy streams by Stefan–Bolzmann's law:

$$E = \sigma T^4, \qquad (3.2)$$

where T is heated body temperature; σ is the Stefan–Boltzmann constant (also Stefan's constant) $5.67 \cdot 10^{-4} W / m^2 K^4$.

Recall that the temperature of the Sun's surface is $T_\odot = 5778K$, its radius is $R_\odot = 6.955 \cdot 10^5$ km, and the Earth' radius is $r = 6.378 \cdot 10^3$ km. The mean distance between the Sun and the Earth is $\rho = 1.496 \cdot 10^8$ km. The radiation stream reaching the globe is proportional to the squared ratio of the solar radius and the mentioned distance $R_\odot / \rho^2$.

The solar energy received by the Earth could be defined as:

$$E_1 = k_1 \sigma T_\odot^4 \pi r^2 \; R_\odot / \rho^2 \qquad (3.3)$$

The IR radiation energy reflected to the Universe is:

$$E_2 = k_2 \sigma t^4 4\pi r^2 \qquad (3.4)$$

In these equalities k_1 and k_2 are the portions of energy received and reflected, respectively, by the Earth.

If we assume the Earth to be without atmosphere, all the solar energy streams would reach its surface. In turn, also all the received energy would be reflected back into the space ($k_1 = k_2 = 1$). In this case, the mean global temperature is to be found using the equality: $E_1 = E_2$, which gives:

$$t = T_\odot \sqrt{\frac{R_\odot}{2\rho}\sqrt{\frac{k_1}{k_2}}} \qquad (3.5)$$

Substituting the numerical values we obtain:

$$t = 5778\sqrt{\frac{6.955\cdot 10^5}{2\cdot 1.496\cdot 10^8}\sqrt{\frac{1}{1}}} = 278K \Rightarrow 5°C .$$

Since the atmosphere ozone layer inhibits the solar ultra-violet radiation, and the global surface reflects to the space a portion of visible light (albedo) (Fig.3.1), the Earth receives only about 70% of the solar energy: therefore, $k_1 = 0.7$. Not taking into account the green-house effect we have $k_2 = 1$ and:

$$t = 5778\sqrt{\frac{6.955\cdot 10^5}{2\cdot 1.496\cdot 10^8}\sqrt{\frac{0.7}{1}}} = 255K \Rightarrow -18°C .$$

This temperature corresponds to a glacial period.

Considering the global heat reflection to be limited by the absorbing windows $k_2 = 0.3$ the temperature would be:

$$t = 5778\sqrt{\frac{6.955\cdot 10^5}{2\cdot 1.496\cdot 10^8}}\sqrt{\frac{0.7}{0.3}} = 344K \Rightarrow 71°C$$

Therefore, if it were truth that the Earth reflects energy by radiation only, its climate catastrophe would have happened at the very beginning.

It is known that the average global temperature is equal to 288 K (+15 ºC). To ensure such temperature, much more powerful heat removal is needed, i.e.:

$$k_2 = k_1 \frac{T_\odot^4}{t^4}\frac{R_\odot^2}{4\rho^2} = 0.7\frac{5778^4}{288^4}\frac{6.955\cdot 10^5{}^2}{4\cdot\ 1.496\cdot 10^8{}^2} \Rightarrow 0.62 \quad (3.6)$$

This value is ensured by two components. A portion of heat (about 30%) is reflected by IR radiation. The second portion comes from the lower layer of the stratosphere. The heat arrives here through convection – with the help of vertical atmospheric air components of the stream, by-passing the zones for absorption of greenhouse gases.

CHAPTER 4.
RADIATION AS A CHANNEL FOR THE GLOBAL HEAT TRANSFER

4.1. IR radiation laws

The relationship between radiation density E, absolute temperature T and wavelength λ is defined by the Planck equation containing an exponential function:

$$u(\lambda,T) = \frac{2\pi hc^2}{\lambda^5 \left(e^{hc/T\lambda k} - 1\right)} \qquad (4.1)$$

where $C_1 = 0.50544 \cdot 10^{-16}$ W/m^2; $C_2 = 1.4388 \cdot 10^{-2}$ m·K; h is the Planck constant; c is the light speed in vacuum; k is the Bolzmann constant.

With Planck's law the Stefan–Bolzmann law is closely connected, which determines the relationship between the temperature source and the total energy passing through a square centimetre of its radiative surface. The radiation density in the infra-red region is determined in compliance with Stefan–Bolzmann's law using (3.2).

4.2. Absorption process

It is known that the free radiation is impeded by molecules of green-house gases that are present in the atmosphere. The essence of the process of radiation absorption can be illustrated by the operation of a solar collector (Fig.4.1, [20]). Such a collector presents a

glazed box containing a water circulation system. Glass is transparent for visible radiation and only partially transparent for infra-red radiation, thus allowing some energy to be accumulated in the collector.

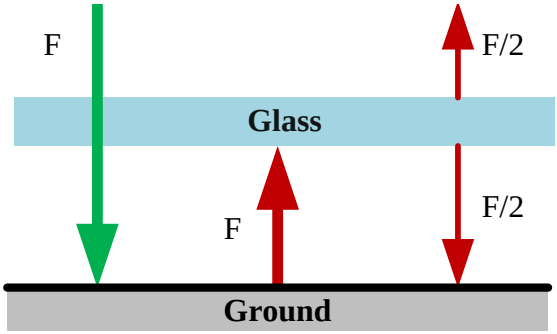

Fig.4.1. Scheme of the solar collector operation

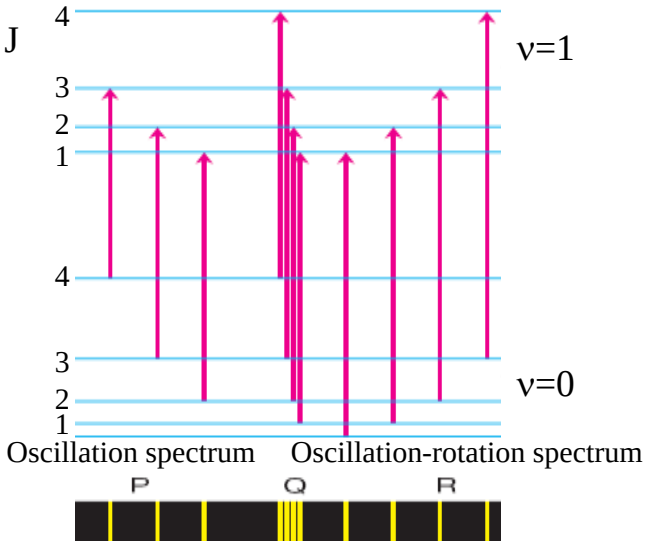

Fig.4.2. Spectral lines of dipole molecules

In the atmosphere, the IR radiation is trapped not in a thin layer but in the depth owing to the presence of molecules with dipole properties. The radiation processes are studied by spectroscopy, from which it follows that to each of the dipole molecules reacting to radiation definite spectral lines correspond Fig.4.2.

This phenomenon of the quantum mechanics, according to which the radiation transmission or absorption occurs, is connected with that similar to resonance.

4.3. Absorption by water vapour molecules

Water vapour molecules under the infra-red radiation experience changes in three energy levels (Fig.4.3).

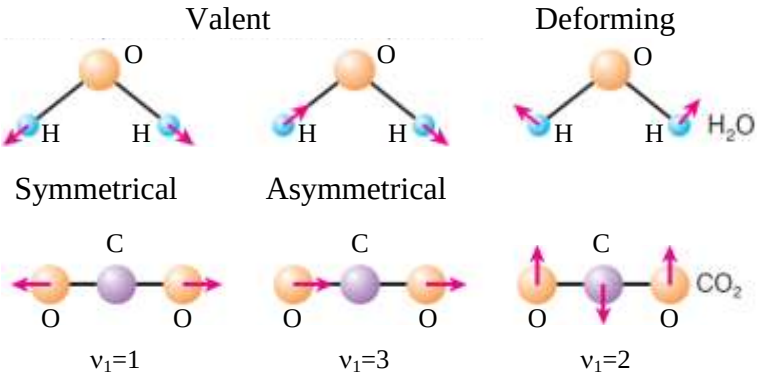

Fig.4.3. Deformations of water and CO_2 gas molecules

The first two – symmetrical and anti-symmetrical deformations of the bonds between hydrogen and oxygen atoms – cause oscillations. The third one is

variation in the angle between the bonds (being 104.5° at rest) followed by rotation. In fact, the molecules in mutual collisions have indefinite motion velocity, *v*, which varies in the $\pm\Delta$ range (respectively, the maximum and minimum velocities being $v+\Delta$ and $v-\Delta$). In compliance with Doppler's effect, the spectral lines extend when responding to different velocities, thus transforming the bands with a profile characteristic of the so-called normal distribution. When such bands are overlapping they form absorption zones.

The properties, which are similar to those of resonance, correspond to definite frequency ranges – "windows". The corresponding absorption zones for water molecules have frequencies that discretely cover infra-red radiation in the following regions: 4.2–4.8; 5.2–8 and 22–70 μm.

The absorption of water molecules almost fully overlaps the radiation in a wide spectral region. As a result, from the whole range of 2-70 μm for radiation it only remains a zone of 8-14 μm [17].

The gap seen in the transparent window corresponds to ozone and, partially, to oxygen molecules, which, at electronic shells being deformed at mutual molecular collisions, acquire weak dipolar properties.

Water molecules in the atmosphere are dominant in greenhouse gases. In the vaporous state their heat absorption is approx. 70%, and absorption by clouds ─

20%. The rest 10% fall on other heat absorbing molecules existing in the atmosphere.

As concerns water molecules in the atmosphere, they are unstable. Under natural conditions, when a cold period begins, water is frozen out, which reduces the heat absorption and favours the onset of a glacial epoch.

4.4. Absorption by carbon dioxide gas

Carbon dioxide, whose molecules possess dipolar properties, is a stable green-house gas. At definite infra-red radiation wavelengths such molecules acquire three types of deformations: unilateral, anti-symmetrical oscillation and oscillation-rotation ones (Fig.4.3), which create a relatively narrow (14–16 μm) absorption window. This wavelength interval is situated in the region with reduced window saturation of the water molecules, whose specific absorption profile is shown in Fig.4.4 [17].

In the figure, to the spectral line consolidation (at 15 μm, the maximum absorption) the Q-zone corresponds, which is saturated. To the rare spectral lines the weak absorption wings R and P correspond (higher and lower frequencies, respectively). In the general view of absorption windows it could be seen that the P wing is overlapping the water absorption zone.

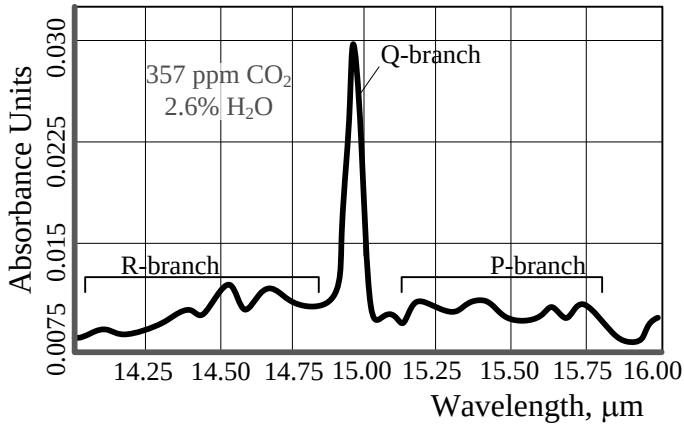

Fig.4.4. The profile of CO_2 absorption

4.5. Zone of transparency for the infra-red radiation

Absorption zones form windows (Fig.4.5) whose effect depends on their saturation.

For water molecules they are saturated in a wide region in which the atmosphere becomes practically opaque. The saturation for water absorption gradually decreases in the 14–22 μm region, and in the 8.6–14 μm region the atmosphere is transparent [18]. Through such windows there leaves a portion of the solar energy accumulated by the Earth (shown in the figure by dark colour).

In Fig.4.6 the IR radiation zones are represented on a linear scale. The figure shows zones of CO_2 absorption and transparent for radiation (grey).

To reveal important properties of the absorption zone for carbon dioxide it is necessary to know the temperature

distribution in the near-Earth space up to the altitudes where the heat transfer proceeds by convection − i.e. up to the stratosphere. This is visualized by Fig.4.7, where the known dependence of temperature on the altitude is presented.

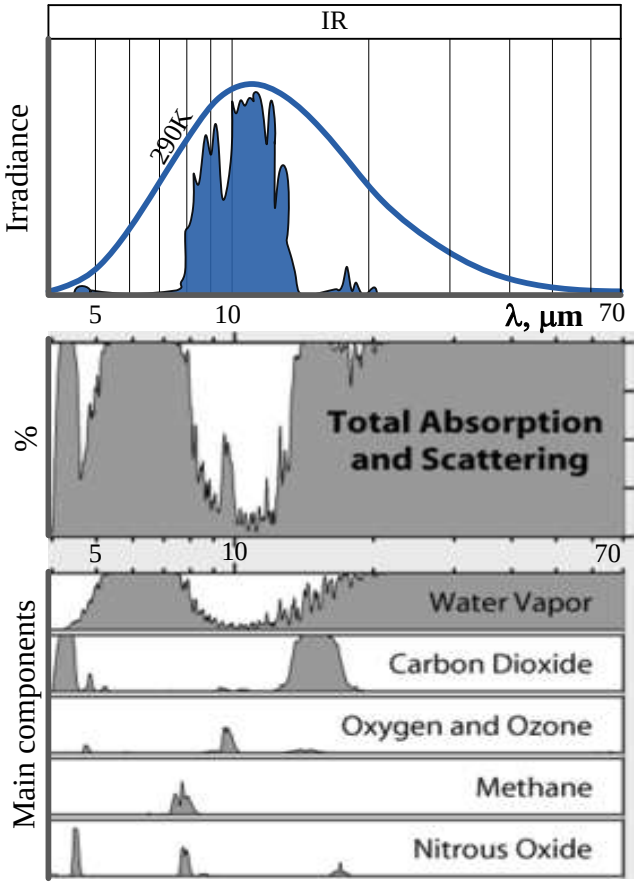

Fig.4.5. a − intensity of global IR radiation; b − total absorption and scattering at different wavelengths; c − absorbtion bands for the main greenhouse

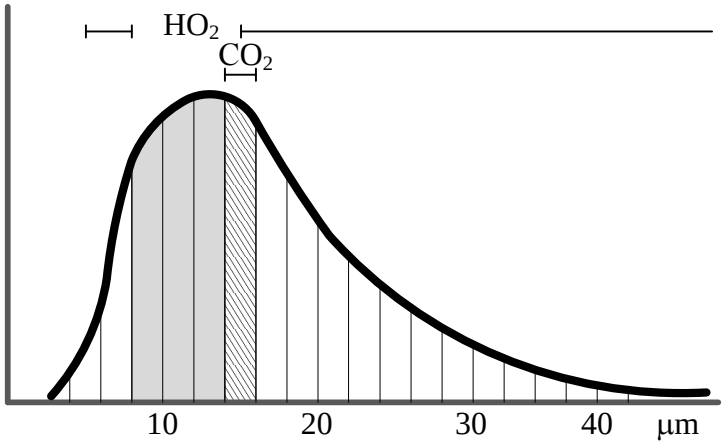

Fig.4.6. The infrared radiation zones on a linear scale

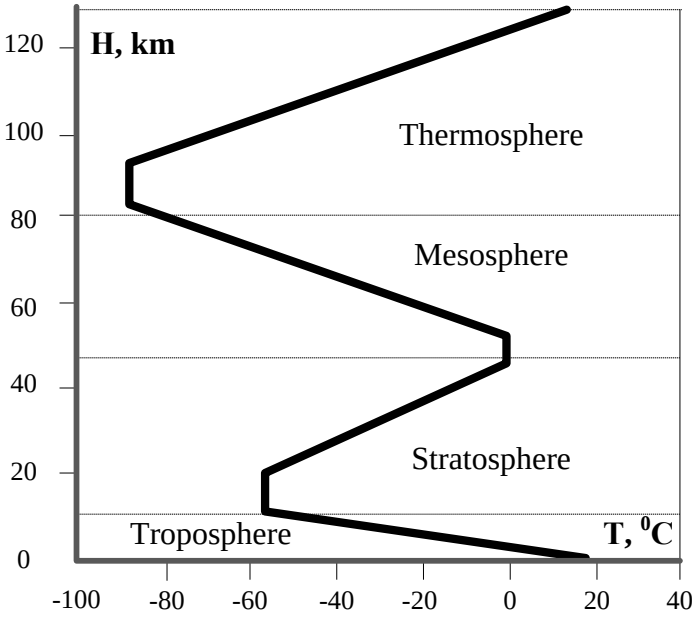

Fig.4.7. Altitude dependence of atmospheric temperature

In the troposphere the temperature decreases with altitude, reaching at the boundary the value of about −50ºC. On the borderline between stratosphere and mesosphere (the intermediate atmosphere stratum at altitudes of 50-85 km) the temperature is gradually increasing up to 0ºC, further decreasing down to −90÷−100ºC. In the thermosphere (the altitudes of 80-300 km) the temperature again gradually increases up to 1300÷2500ºC.

The released heat depends on the absorption zones, global surface temperature, and the atmosphere altitudes.

In Fig.4.8, the temperature record is shown (as of 05.05.1970, performed by satellites: (a) over Sahara and (b) over Arctic) against the background of lines corresponding to different temperatures (K) in Planck's equations (as shown in Fig.3.2, [17]) [18].

The satellite records were made at different wavelengths. The range of 8-14 μm is the zone of transparency for infra-red radiation. Beyond the boundaries of this zone the heat is transferred by convection of low amplitude, uniformly in the domain of IR radiation.

The arrow in Fig.4.8 (a) points to the CO_2 absorption zone for the wavelengths of 14-16 μm. It is obvious that the primary radiation in this zone is absent − and the radiation temperature is sharply down to 218K (-55ºC) corresponding to the conditions in the lower stratosphere layers. Respectively it is the secondary radiation which

is delivered to this height with the vertical convective masses of air flows. Possibly, the CO_2 absorption zone is practically opaque for radiation.

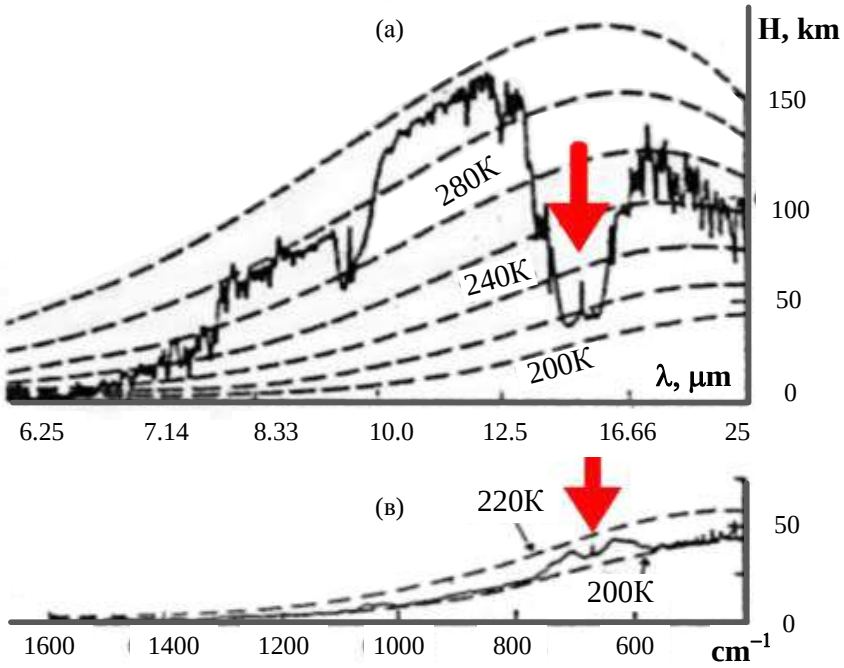

Fig.4.8. Reflection radiation from the Earth (measured by satellites over Sahara (a) and in polar region (b))

The elevated temperature in Fig.4.8 (b) is caused by intense convective streams reaching the northern latitudes.

4.6. Response of the radiation channel to temperature changes

When the temperature is changing in response to an external cause, the radiation channel, acting in the zone of transparency in compliance with Stephan-Bolzmann's law, enhances the convective heat transfer. This process is characterised by a 4^{th} order parabola (shown in Fig.4.9, curve 1).

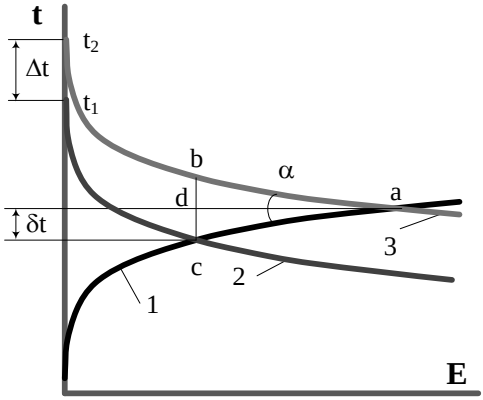

Fig.4.9. The structure of the radiation channel behaviour at a temperature change owing to an external cause

As this takes place, the temperature of the Earth surface decreases in accordance with another parabola (curve 2), which is specular (mirror-like) with respect to the first one. The established state corresponds to the intersection point of these characteristics. To the temperature change by Δt owing to an external cause the characteristic 3 corresponds. The situation is elucidated by the isosceles

area *abc*. The *ad* line is the bisector of angle α, and, consequently, it bisects the base *bc*. As a result, $\delta t = \Delta t / 2$, which means that the response of the radiation channel to the temperature change owing to the external cause reduces this change by half.

CHAPTER 5.
THE HEAT REFLECTION BY CONVECTION

5.1. The regularities of convection

Convective air streams in the atmosphere are formed by masses of warmed and incompact air that is vertically ascending from the Earth surface and, simultaneously, by descending masses of colder and denser air. The velocity of such vertical streams reaches 20–30 m/s. Energetic convective vertical streams, being a component of the total air circulation, permeate the whole atmosphere and reach the stratosphere, thus playing an important role in the heat exchange between the atmospheric layers and fulfilling the function of heat transfer into the Universe.

The heat removal by free convection of atmospheric air flows per area unit proceeds according to Newton's law:

$$E_c = \alpha \ T_1 - T_2 \qquad (5.1)$$

where T_1, T_2 are the temperatures on the global surface and the lower layers of stratosphere, K; α is the convection heat transfer coefficient, W/m^{2}K.

The average global heat reflection is:

$$E_c = \alpha T^4 \pi r_e^2 \qquad (5.2)$$

This portion of heat is delivered by the convective channel, through which the heat is transported by powerful vertical air streams to the upper troposphere layers not containing water vapour molecules, by-passing the water absorbing windows. From there it is dissipated in the space, at the infra-red radiation wavelengths corresponding to cooled media.

The infrared radiation is transferred only through the transparent windows; in contrast, convective flows are distributed uniformly over the whole radiation range, with the convection effectiveness increasing with temperature (Fig.5.1).

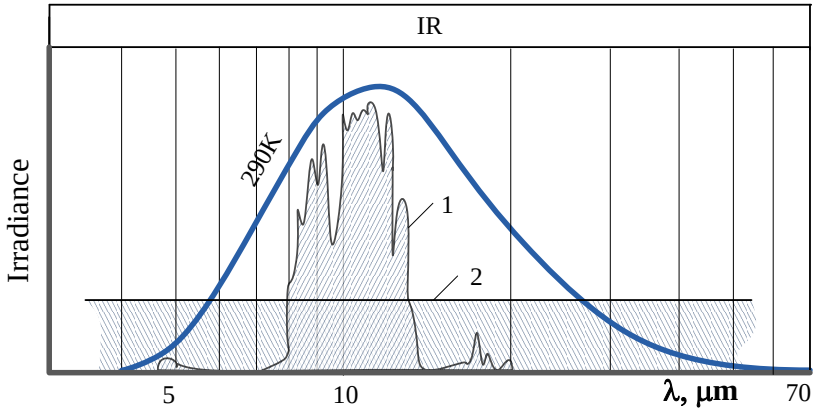

Fig.5.1. Zones of global heat removal: (1) by radiation, (2) by convection

If, for example, owing to solar activity variations the temperature grows (which was observed during the past century) the transmittance of the convective channel

increases proportionally to the variation in temperature thus causing its decrease.

Taking into account the calculations performed in Ch.3, the temperature change owing to convection is:

$$\frac{\Delta T}{\Delta E} = \left|\frac{72-15}{30-62}\right| = 1.73^{\circ} C / E_{\%} .$$

Since the ratio between the radiation and convection channels is 30/32%, these two channels for energy transfer are practically equivalent.

5.2. The convective air flows

The convection under consideration, i.e. a planetary horizontally-vertical air circulation, can be presented in the form of three air motion rings as follows [23].

First planetary circulation ring, in which the heat exchange proceeds between the warmed equator and cold poles, with heat transfer by vertical air streams to the upper layers of troposphere (see Fig.5.2). Having given up heat, the air is descending, streaming back towards the equator. Owing to the Earth rotation, these streams in Northern Hemisphere are east-bound, and in Southern Hemisphere – west-bound.

Second planetary circulation ring, which in these latitudes is formed by the accumulated air masses creating a zone of elevated pressure. From there the air masses are streaming in two directions determined by

the Earth rotation (Coriolis') forces. A proportion of the cooled air mass turns back to the equator, forming north-eastern winds (trade-winds) closing the second circle.

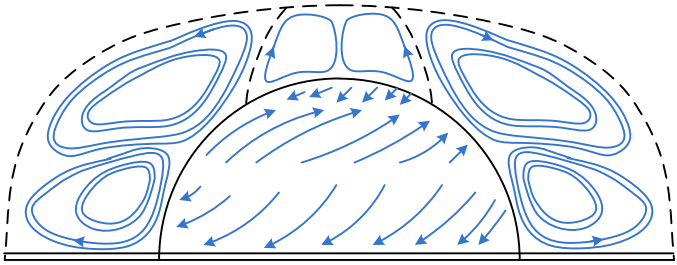

Fig.5.2. Diagram of air streams in the atmosphere

Third planetary circulation ring is formed by a second portion of the air mass that continues to move in the northern direction, shifting to the east under the influence of Coriolis' forces and forming the south-east and east winds. In high latitudes the air, having been cooled, descends and streams south, assuming a western direction of the motion. Having met with the air from temperate latitudes it ascends, thus closing the third circle.

In reality, the described picture is influenced by the dry land's relief and oceanic surfaces. Such a land is rapidly heated up in summer, acting as a cooler, while the ocean possesses a greater inertia, and is functioning as a heater. In winter an opposite picture is observed. Therefore the whole picture is complemented by seasonal influence in

the form of monsoons, which in winter and in summer blow in opposite directions.

5.3. Characteristic curves of the convection channel

These curves are shown in Fig.5.3. Curves (1) characterize the temperature fall at increasing global heat release corresponding to temperatures $T_1;T_2;T_3$ under different conditions. Curve (2) corresponds to the relationships $T = f\ E$, where E is global heat energy.

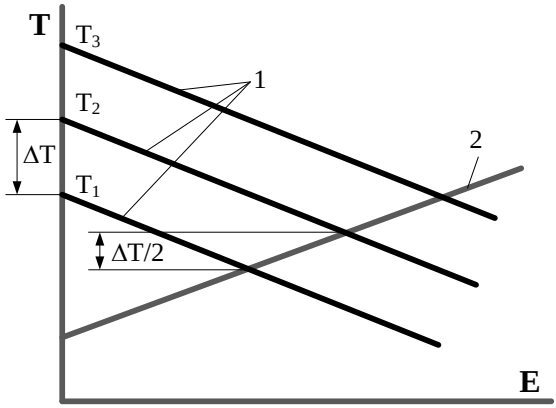

Fig.5.3. Characteristic curves of radiation (1) and convection (2) channels

The equilibrium is established at the intersection points of the curves. The essence of the process is as follows. When the global surface temperature rises by ΔT, in compliance with Newton's law the temperature variation decreases by half $(\approx \Delta T / 2)$.

5.4. The inertia of the convective process

The convective heat transfer is an inertial process with a time constant that is commensurable with the years in which the seasonal variations are equalized. A notion about the inertia of a convective channel could be received when studying, e.g., the changes in the cyclic phase of integral river waterflows connected with solar processes (Fig.5.4).

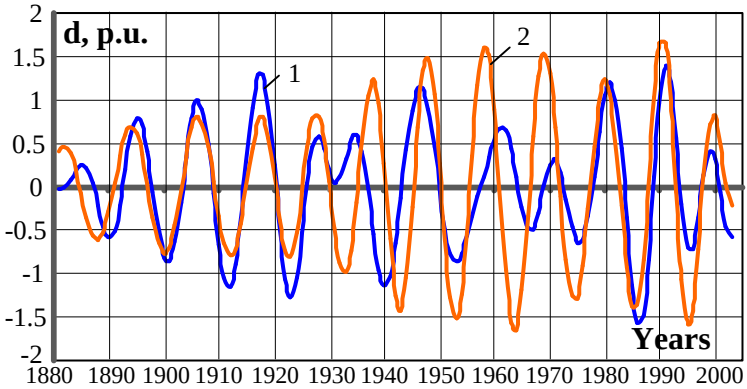

Fig.5.4. Phase changes of river waterflows: 1 – integral value of the Daugava river waterflow; 2 – value of the solar activity

Of course, such fluctuations of a river flow occur after a considerable time, which is connected with oceanic water evaporation, precipitations (that may happen far enough), discharge of ground waters, and so on.

It was mentioned above about a phenomenon − not quite understandable − of the temperature phase change in 1910, which afterwards, 55 years later, was self-

removed. It seemed therefore interesting − is there a like phenomenon also in the river waterflows? There is evidence that a phase change of river waterflows occurred in 1930, i.e. 20 years after the event of 1910 (Fig.5.4).

This could be explained by a long-lasting stationary process of climate change that should have taken place in this case.

This phenomenon could be a subject of further investigation by specialists.

5.5. The effectiveness of the radiation and convection channels

The interaction of radiation and convection channels is shown in Fig.5.5.

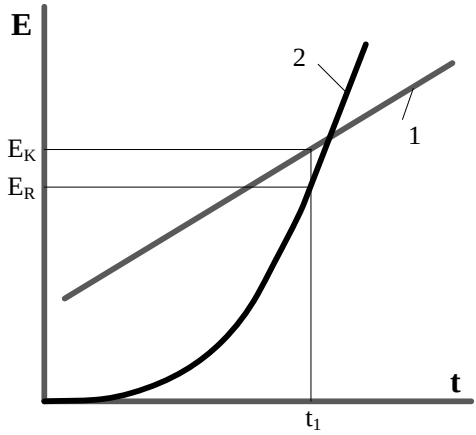

Fig.5.5. Interaction of convection (1) and radiation (2) channels

It is seen that the radiation channel (2) reacts to the temperature very actively; nevertheless, being limited mainly by the absorption of water moleculas this channel turns out to be practically saturated and opaque for infrared radiation.

Not concentrating our attention on the local and short-term features, the system maintaining the global temperature at the level +15 °C, is shown structurally in Fig.5.6, which approximately characterizes the factors influencing the climate of the Earth.

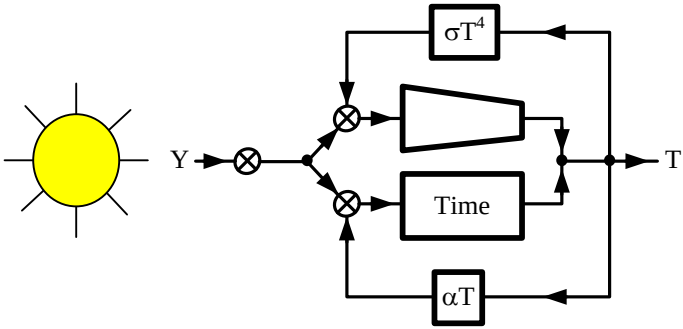

Fig.5.6. Hypothetical structural diagram of the global heat transfer

In this figure, parameter *Y* describes the solar activity variation cycles influencing the global temperature. The Earth appears as the object of temperature variations provided by two channels for heat removal. First of them is an inertialess channel for infra-red radiation, which, responding to temperature, removes radiative heat through the limiting absorptive windows. The static characteristic curve of this channel, σT^4, in practice is

essentially limited. However, this channel is restricted by close to saturation absorption of green-house gases; acting in a narrow channel of transparency in the range 8-14 μm on the background of the common IR region (2-70 μm), it reflects only half of the heat received from the Sun. As a result, the radiation channel, acting at the limit of transmittance, turns out to be practically passive.

The second channel is a two-level (convective-radiative) one. This channel transfers unlimitedly, by convection, the heat to higher atmosphere layers not containing water molecules, by-passing the mentioned limiting absorptive windows, and from these layers the heat is transferred into the space by radiation, within the range of wavelengths corresponding to cooled environment.

5.6. Absorption zones for other green-house gases

The location of absorption zones for other green-house gases on the scale of infra-red radiation waves also deserves attention (Fig.4.5). If they were located within the transparency zone, this latter would be additionally narrowed.

A narrow zone of ozone absorption and of dynamic state of oxygen atoms in the process of their deformation at collisions is originally located in the centre of the transparency zone, thus somewhat limiting the convective heat transfer by the primary radiation.

The absorption zone for methane appears to be located on the high-frequency bound of the transparency zone beyond its limits. As concerns the absorption zone for nitrogen oxides, it coincides with the absorption zone for molecules of water and carbon dioxide gas. If this zone is shut off, these molecules also appear to be beyond the transparency zone.

CHAPTER 6.
THE INFLUENCE OF CARBON DIOXIDE ON THE GLOBAL CLIMATE

6.1. The CO_2 structure on the Earth

It is known that on the Earth in various cycles 150 billion tons of carbon are circulating. Its mass in billion tons is (Fig.6.1):

- in the middle oceanic layers 38100;
- in the near-bottom oceanic layers 150;
- in the superficial layers 1020;
- in sea animals 3;
- in organic oceanic residuals 700;
- in plants 610;
- in soil humus 1580;
- in the atmospheric carbon dioxide 750.

From the carbon balance it follows that the main proportion of the circulating carbon is in oceans (about 98%); as concerns the atmosphere, its amount is only 2%. As a result of soil oxidation the annually produced carbon amount is $102 \cdot 10^9$ tons, and owing to fossil fuel combustion - $6 \cdot 10^9$ tons. The carbon amount annually absorbed by plants in the photo-synthesis processes is $100 \cdot 10^9$ tons.

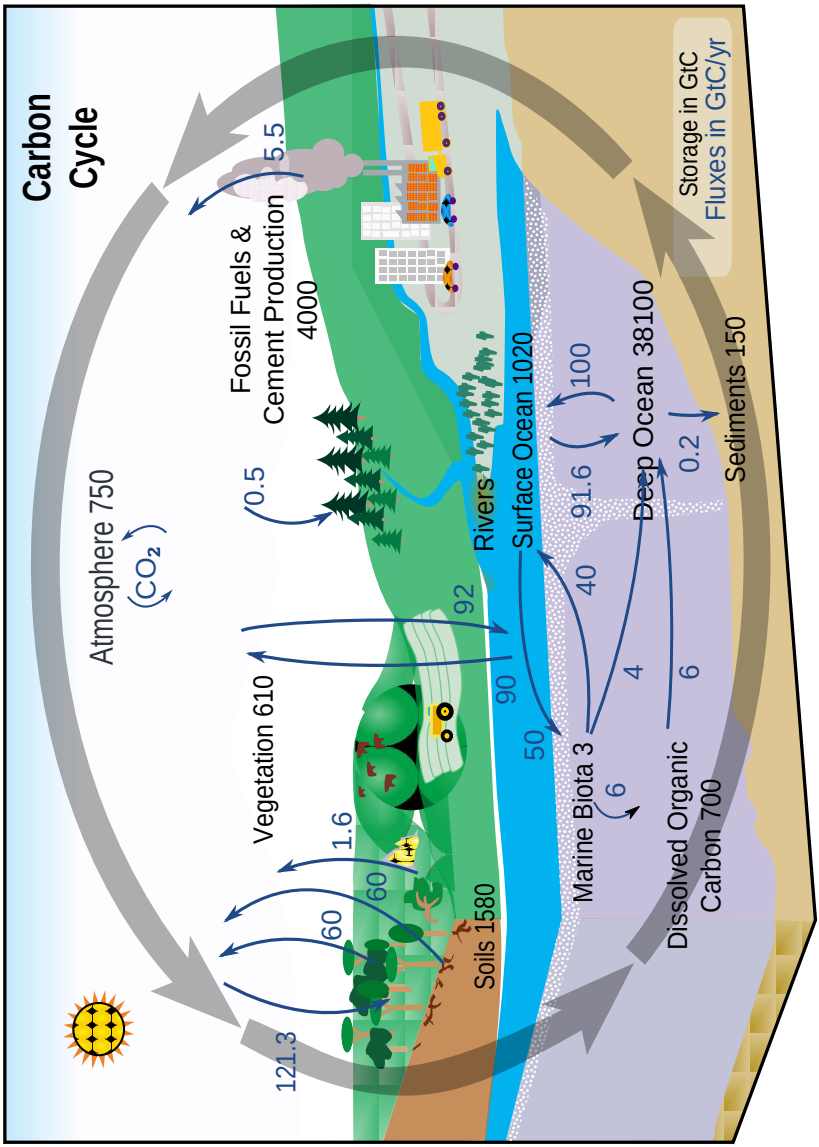

Fig.6.1. Carbon cycle

6.2. The dynamic of carbon dioxide

Fig.6.2 shows the interrelation between the amount of carbon dioxide dissolved in water and the temperature.

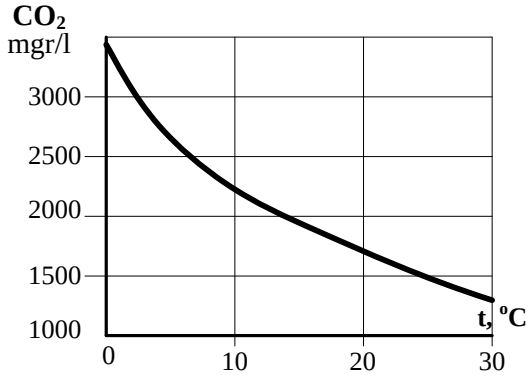

Fig.6.2. Absorption capacity of CO_2 gases in water depending on temperature at the pressure 0.1 MPa (≈1 atm)

We can derive the factual relationships of dynamic equilibrium in the nature from the data for 420 thousand years (a period of four glacial epochs) obtained from the ice cores drilled in Greenland and Antarctic glaciers. These data are shown in Fig.6.3 [19], where it is clearly seen that between the temperature and the specific weight of atmospheric carbon dioxide a dynamical equilibrium exists. With temperature rise, the carbon dioxide is released off from the ocean to the atmosphere. At a temperature fall, the excessive carbon dioxide returns into the ocean, although with some delay. Consequently, the cause of variations in the CO_2 amount in the atmosphere is temperature as the primary factor,

while the effect − the amount of carbon dioxide in the atmosphere that is released from oceans [15].

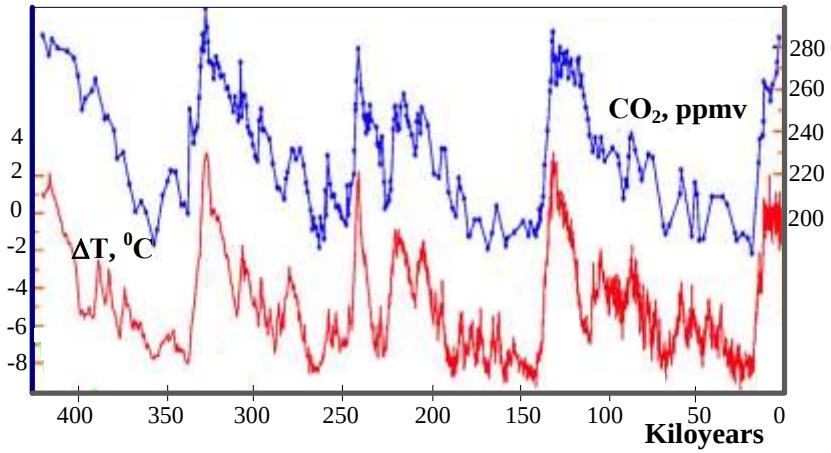

Fig.6.3. The temperature and atmospheric CO_2 relationships in glacial epochs (the data for 420 thousand years)

To avoid contradictory conclusions, the secondary phenomena should be separated from the primary ones. From the above it follows that the primary factor (cause) is the natural temperature change affected by the processes going on the Sun, whereas the secondary one (consequence or effect) – by release of CO_2 gases into the atmosphere (Fig.6.2 and Fig.6.3).

6.3. The influence of feedbacks

The external cause of temperature changes is associated with the heat balance resulting from the processes happening on the Sun. This balance is established by

means of the global heat reflection into the cosmic space.

The character of the temperature change process depends on the type of arising feedbacks. The positive feedbacks enhance the deviations from the equilibrium state, whereas the negative feedbacks are favourable for state stabilization.

6.3.1. Positive feedbacks

Reflection of visible light from the polar surfaces. One of the phenomena possessing a positive feedback is the direct reflection of light by the polar surfaces of the Earth. The temperature rise owing to natural causes is accompanied by reduction in their area, and, consequently, by reduced reflection of heat. As a result, the temperature is rising still more.

Zone of transparency for CO_2 absorption. Another factor of positive feedback that manifests itself in the time of glacial epochs is decrease in the specific weight of carbon dioxide in the atmosphere at temperature falls. As seen from Fig.6.3, at partial CO_2 absorption from the atmosphere by oceanic waters its specific weight decreases there to the value of 200 ppm. In such periods the transparency increased in the (14÷16) μm zone, which led to additional heat transfer and temperature fall. When this took place, the specific weight of CO_2 in the atmosphere became 100 ppm less.

Meanwhile, owing to the rise in the CO_2 specific weight in atmosphere, its minimum value in the future will also increase − presumably up to 300 ppm; along with this, the transparency of the absorption zone and the role of this positive feedback will decrease. Possibly, this would limit to an extent the depth of temperature fall.

6.3.2. Negative feedbacks

Reflection of visible light from the clouds. The temperature rise under the influence of external factors is favourable for intensive water evaporation from oceans and enlargement of cloudiness. As this takes place, the visible light reflection by light-coloured surfaces of clouds increases, which via the negative feedback reduces the temperature and stabilizes it. At temperature changes, the phenomena associated with the polar areas and evaporation become mutually compensated to a certain degree.

Response to the temperature rise. The radiation in the transparency zone and the convection in the whole region of infra-red radiation, responding to the temperature rise on the Earth surface, increase the release of heat, thus impeding the temperature change. This shows up in the form of negative feedback favouring the temperature stabilization.

6.4. Influence of climate changes on the oceans

The short-term temperature elevations − i.e. those arising in every millennium due to natural causes − were accompanied by intense thawing of polar glaciers. The events happening in the inter-glacial period (at least during 5000 years) do not provide grounds for the suggestions that on the European continent there have been serious changes of the kind. Therefore, the processes of the past do not give grounds to any anxiety about a probable change in Gulf Stream's course which could lead to catastrophic climatic consequences for Europe − at least in the foreseeable future.

It is known that the temporary temperature elevations of oceanic surfaces that arise periodically in the southern latitudes are accompanied by enhanced florescence of phytoplankton, which after vegetation sinks into depths. Its decomposition is associated with consumption of the oxygen dissolved in oceanic waters, which, along with their worse vertical stirring, depletes these waters of the oxygen content necessary for vital functions of the oceanic flora and fauna. This is connected with partial destruction of corals and other organisms and with migration of mobile sea fauna in the direction of Polar Regions, whose waters are richer in oxygen. It is believed that, when such periods of extreme temperatures are over, the life in oceans has an opportunity to recover.

Of importance is the issue as to the absorption of carbon dioxide by oceans. Its quantity there depends on the temperature. Therefore, the products of combustion of organic fuels are not absorbed by oceanic water, so their amount, being accumulated in the atmosphere, increases.

One more question is important: whether or not a portion of such emitted products is additionally absorbed by ocean under the influence of an excessive their quantity in the atmosphere. In this case a rise in the acidity could be expected, which deserves attention.

CHAPTER 7.
THE CO_2 RELATED TEMPERATURE CHANGE

7.1. The quantitative CO_2 influence on the temperature

At a small specific weight of carbon dioxide the radiation mainly penetrated through its absorption zone (14÷16 μm) in compliance with Stephan-Bolzmann's law. As the specific weight was increasing, the transparency of this zone decreased, and, therefore, the heat transfer was also less. As long as the decrease in the heat transfer was considerable, this was accompanied with a rise in the temperature, to which the radiation and convection channels responded by halving its change.

Then, as specific weight of carbon dioxide increases, the absorption zone becomes saturated − now to large changes in the CO_2 specific weight only minor changes in the heat flow correspond; as a consequence, this flow should practically cease (Fig.7.1).

The issue as to the influence of CO_2 amount in the atmosphere on the temperature change is thus reduced to the determination of the opaqueness degree of the primary radiation absorption zone.

It is important to find out at what specific weight G of CO_2 molecules this would occur (if has not yet occurred in practice).

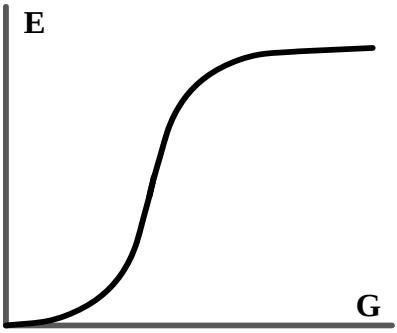

Fig.7.1. Dependence of the heat transfer on the specific weight of carbon dioxide

It is known that the temperature change in the saturation zone is approximately corresponding to the logarithmic function $t = \log G$ (Fig.7.2).

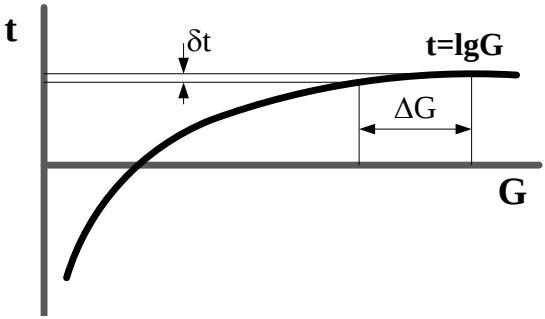

Fig.7.2. The plot of common logarithmic function

Applying a linear approximation to the saturation zone, we obtain the temperature change as $\delta t = \beta \Delta G$, where β is the coefficient of proportionality, $^{\circ}C / ppm$. In turn, this coefficient decreases with increasing G, and in the limit approaches zero. Accordingly, δt also becomes equal to

zero. As this occurs, the temperature change caused by further increase in the CO_2 specific weight will stop.

From the data of measurements performed in 1970 with the help of satellites (Fig.4.8) it follows that the primary radiation in the absorption zone at the CO_2 amount of 300 millionth fractions is practically absent. Consequently, by then this zone had in fact been opaque for it.

True, within the limits of this zone there is radiation at the temperature of 218K (–55°C). This indicates that the heat originates not from the Earth surface but from the upper layers of troposphere, to which it is delivered by convective airflows.

Dr. Heinz Hug (Wiesbaden, Germany) [22] has considered the problem applying a physical model under laboratory conditions. From his experiments and the related calculations it was established that at a doubled amount of carbon dioxide in the atmosphere (from 357 to 714 ppm) the temperature − owing to the primary radiation − increases by 0.17%, since the remaining elements of partial transparency are filled along the boundaries of the absorption zone (shown as black spots in Fig.7.3 [22]).

As this takes place, the opaqueness for radiation will be:

$$100\% - 0.17\% = 99.83\%.$$

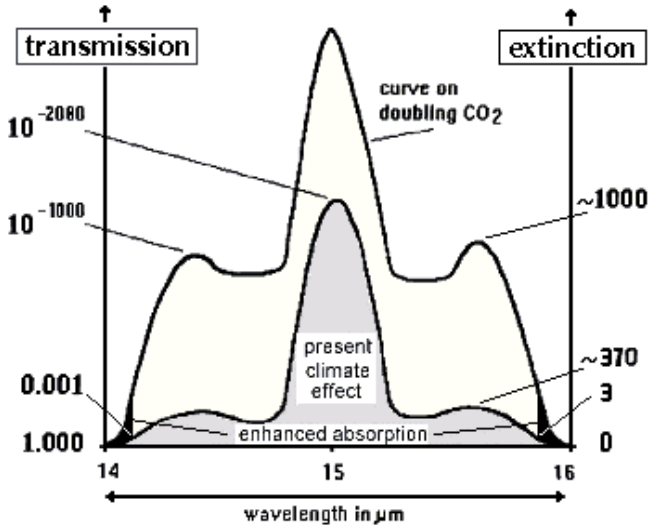

Fig.7.3. The apsorption span for doubled CO_2 (from 357 to 714 ppm) [22]

The heat flow in the interval along P-R absorption branches (Fig.4.4) in logarithmic coordinates for the initial specific weight of CO_2 in atmosphere corresponds to a 370-fold reduction in transparency. At the specific weight of 714 ppm the transparency decreases 1000 times (Fig.7.3). In reality this is tantamount to the opaqueness.

Apparently, the result obtained needs some corrections associated with the relations between radiation and convection. The first coefficient accounts for the share of the heat given up through radiation (coefficient $k_r / k_c + k_r$). The second one − for the response of

radiation and convection to the temperature rise that halves this change. Thus we have:

$$\frac{k_r}{2(k_r + k_c)} = \frac{30}{2(30 + 32)} = 0.24$$

where $k_r; k_c$ – the shares of the energy reflected by radiation and convection, respectively.

Consequently, the opaqueness for the primary radiation will likely to reach 99.96%, therefore the carbon dioxide at its current specific weight in the atmosphere would not practically affect the temperature change.

In this connection another problem is topical from the viewpoint of vital functions − that of the limiting specific weight of carbon dioxide which will be present in the atmosphere after burning the main reserves of fossil fuels, especially as refers to the development of commercial production of methane-hydrates.

As concerns the global climate change observed today, it could be stated, based on the data considered, that this change is of temporary character, and is directly associated with the recurrent extremal growth in the solar activity, which takes place today and is short-term. Such periods of elevated solar activity arise regularly, with intervals of about one thousand years.

7.2. Forecasting of the probable temperature changes

As a result of regular cycles in solar activity variations, the millennia of elevated global temperature are followed by those of its decrease.

As analogues for the future climate change process, four its images displayed in Fig. 2.1 could be employed. These images allow for a suggestion that during the XXI century a first phase of cold snap could be expected (shown in Fig.7.4 between 1-2 curves). Then, in the XXII century this temperature fall will proposedly go on, after which the temperature changes will depend more on the character of 200-300-year cycles of solar activity.

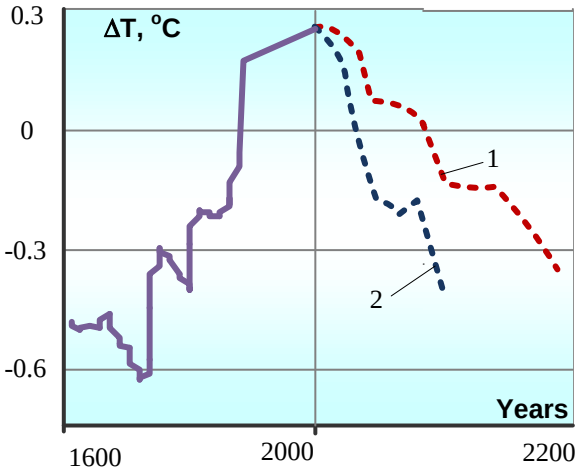

Fig.7.4. An expected cold snap in the XXI-XXII centuries

The analytical approach to the problem of climate change does not deny the basic principles of the rational use of energy, improvement of the efficiency of power generating equipment and distributed co-generation and implementation on a large scale of the alternative energy sources in order to eliminate the environmental pollution by such harmful to the health emissions as sulphur dioxide, nitrogenous oxides and dusts from fossil fuel combustion.

As concerns the climate change owing to the cyclic solar processes, it is clear that the temperature, having reached a maximum, by the middle of the current century will have fallen analogically to processes that repeatedly occurred on the Earth.

In view of the inter-glacial period dynamics, it is possible that in the next millennium the temperature will fall deeper than in the past millennium (during the so-called Small Ice Period (Fig.2.3).

CONCLUSIONS

1. To investigate the causes of climate change the spectral analysis based on discrete wavelet transform has been carried out for such processes as river waterflows, global temperature and solar activity variations. The analyzed processes, retaining their natural character, are divided into the components which in pairs (waterflow-sun, temperature-sun) can be juxtaposed with each other, and, having established a close analogy between them, to determine unambiguously the cause and the effect.

2. For all frequencies (periods) a coincidence has been obtained for the character (cyclicity) of global and solar processes.

3. The mean global temperature of ~15 ^{o}C is ensured by 62% reflection of the heat obtained from the Sun. A half of this heat reaches the periphery of atmosphere via convection with powerful air streams by-passing the zones of absorption for green-house gases in compliance with Newton's law. The remaining heat leaves this cooled and rarified environment and goes to space in the form of radiation of corresponding wavelengths.

4. The temperature variation with a growth in the specific weight of CO_2 in the atmosphere is insignificant owing to the flatness of this dependence caused by saturation of the process at which the absorption zone becomes practically opaque for radiation.

5. All the said does not underestimate the topicality of the problem of climate change; nor it minimizes the usefulness of attempts to raise efficiency of energy production and its rational use as well as of the measures towards elimination of harmful exhausts into the environment.

BIBLIOGRAPHY

1. Barkans J., Zicmane I. "Peculiarities of annual flows of World`s rivers" (with D.Zalostiba participation (8.3.Ch.)), *World Energy Council, Nacional Committee of Latvia. Riga: RTU,* 210p. (2005).

2. Vitjazev V. "The wavelet analysis of time series: Textbook", *S.Peterburg University,* 58 p. (2001) (in Russian)

3. Astafjeva N.M. "The wavelet analysis: theoretical foundations and application examples", *Uspehi fiz. Nauk,* vol.166, No.11, p. 1145-1170 (1996) (in Russian)

4. Polikar R. "Introduction in the wavelet transformation", *Iowa State University,* 50 p. (2003)

5. Brukner E. "Klimaschwankungen", *W-Olmutz* (1890)

6. Burroughs W.J. "Weather cycles: real or imaginary?", *Cambridge: Cambridge University Press,* 317 p. (2003)

7. Hathaway D.H., Wilson R.M., Reichmann E.J. "A synthesis of solar cycle prediction techniques", *Journal of geophysical research,* vol.104, No.A10, p. 22,375-388 (1999)

8. Data of sunspot available at ftp://ftp.ngdc. noaa. Gov /STP /SOLAR_ DATA /SUNSPOT_ NUMBERS/YEARLY.PLT

9. Barkans J. "Climate change and energy", *Journal „Energy and World"*, vol.3 (2007) (in Latvian)

10. Barkans J., Zalostiba D. "View of climate changes based on the wavelet analysis of Solar intensity", *Latvian journal of physics and tehnical sciences*, vol.1, p. 3-11 (2008)

11. Barkans J., Zalostiba D. "Climate as a result of the Earth heat reflection", *Latvian journal of physics and tehnical sciences*, vol.2, p. 29-39 (2009)

12. Data of temperature anomalies available at http://www.cru.uea.ac.uk/cru/data/temperature/ hadcrut3gl.txt

13. Polikar R. "Introduction in the wavelet transformation", *Iowa State University*, 50 p. (2003)

14. Abdussamatov H.I. "On long-term variations of the total irradiance and decrease in global temperature of the Earth after a maximum of XXIV cycle of activity and irradiance", *Izvestija of Crimean Astrophysical Observatory*, vol.103, No.4, p. 292-298 (2007) (in Russian)

15. Dansgaard W. "Stable isotopes in precipitation", *Tellus*, vol.16, No.4, p. 436-468 (1964)

16. Epstein S. "Variations of the $^{18}O/^{16}O$ ratios of fresh water and ice", *National Academy of Sciences. Nuclear science Ser.*, Report 19, p. 20-25 (1956)

17. Chumichow S.A. "Climate of golocen", *Institute of low temperature science. Hokkaido Unversity, Sapporo* Japan 060-0819 (2002)

18. Grootes, P.M., and Stuiver, M. "Oxygen 18/16 variability in Greenland snow and ice with 10^3 to 10^5-year time resolution", *Journal of Geophysical Research*, p. 102:26455-26470 (1997)

19. Petit, J.R., et al. "Vostok Ice Core Data for 420,000 years" *IGBP PAGES/World Data Center Paleoclimatology Data Contribution Series* #2001-076. NOAA/NGDC Paleoclimatology Program, Boulder CO, USA (2001)

20. Tonkov M.V. "Greenhouse effect Spectroscopy", *Sorosovsky obrazovatelny zurnal*, vol.7, No.10 (2001) (in Russian)

21. C.B.Farmer, R.H.Norton. "IR Spectrum of Sun and Earth Atmosphere", *Planetary and Space Science*, vol. 40, iss.4, p. 570-570 (1989)

22. Dr. Heinz Hug. "The climate catastrophe - A Spectroscopic Artifact", available at http://www.john-daly.com (1998)

23. Fedotova V.D. "Common circulation of atmosphere", available at http://www.primpogoda.ru /articles/ (in Russian).